

5'LysTTT tRNA fragments support survival of botulinum-intoxicated neurons by blocking ferroptosis

Arik Monash^{1,2,3} , Nimrod Madrer^{2,4} , Shani Vaknine Treidel^{2,4} , Ofir Israeli⁵ , Liad Hinden³ , David S. Greenberg² , Joseph Tam³ , Osnat Rosen⁶ , and Hermona Soreq^{2,4} 

Botulinum neurotoxins (BoNTs) block cholinergic signaling at neuromuscular junctions, inducing transient muscle paralysis while avoiding neuronal death. However, the mechanism(s) underlying these dual features are yet unknown. Here, we report accumulation of 5'Lys transfer RNA fragments (tRFs) in both BoNT/A-intoxicated cultured human neuroblastoma cells and submandibular glands from BoNT/A-intoxicated rodents. Importantly, we show that 5'LysTTT tRFs balance ferroptosis by cointeracting with the RNA-binding ferroptosis-inducing protein HNRNPM and the 3' untranslated region of the ferroptosis-inhibiting CHAC1 mRNA. Moreover, approximately 20% of the BoNT/A-induced tRFs shared an 11-nucleotide-long LysTTT and LysCTT tRFs-included motif, CCGGATAGCTC, which may target transcripts containing complementary sequences, including the UNC5B transcript that can regulate cell survival. Collectively, the multiple regulatory roles of tRF-5'LysTTT and the shared repetitive motif reveal mechanism(s) supporting the survival of cholinergic neurons under BoNT/A exposure. This understanding may predict the development of novel BoNT/A therapeutic avenues for treating diverse neuromuscular disorders and BoNT/A cosmetic procedures.

Genomic Psychiatry (2025), 1–17; doi: <https://doi.org/10.61373/gp025a.0047>

Keywords: Botulinum, ferroptosis, neurons, neuromuscular junction, paralysis, small noncoding RNA, tRNA fragments

Introduction

Botulinum neurotoxins (BoNTs) are the most potent biological toxins known to humans, with an estimated lethal dose of approximately 1 ng/kg (1). These toxins are the causative agents of botulism, a severe and potentially fatal neuromuscular illness affecting both humans and animals (2). Paradoxically, BoNTs also form the basis for a variety of cosmetic and therapeutic applications (3). Produced by anaerobic *Clostridium* bacteria, BoNTs are initially synthesized as single-chain precursor proteins, which are subsequently processed into a 100 kDa heavy chain and a 50 kDa light chain. Different *Clostridium* strains produce seven BoNT serotypes (A to G) (4), of which serotypes A, B, E, and rarely F, are associated with human botulism. Annually, a few hundred cases of infant or adult intestinal botulism are reported worldwide (5). Mechanistically, BoNTs act by entering peripheral cholinergic neurons through a multistep cellular intoxication process that culminates in the cleavage of core SNARE proteins. This interrupts acetylcholine (ACh) trafficking and release at the neuromuscular junction (NMJ), leading to paralysis (6, 7). Infants are particularly vulnerable to botulism, and since 1979, infant botulism has been the most commonly diagnosed form of this poisoning in the United States (8). Neurological symptoms in infants are similar to those in adults, but are often overlooked because infants cannot verbalize their discomfort. The most common sources of infant botulism are contaminated honey and environmental exposure (9, 10). From 2000 to 2019, infant botulism represented 71% of the 3241 human botulism cases detected in the United States (11).

While BoNT/C and BoNT/E serotypes have been shown to cause neurodegeneration in both cultured neurons and live mice (12, 13), BoNT/A does not induce neurodegeneration despite its similar ability to block synaptic vesicle exocytosis and cleave the SNAP25 protein (albeit at different positions from BoNT/E) (13). The sustained neuronal survival observed under BoNT/A intoxication has enabled its therapeutic applica-

tion at picomolar or higher concentrations to induce prolonged flaccid paralysis (14). This effect is utilized in treating disorders such as dystonia, hyperhidrosis, and essential tremors (15). However, the underlying mechanism of action remains largely unexplained. Subsequent studies identified certain proteasome enzymes as key regulators of the duration of post-BoNT/A effects (16, 17) with some analyses focusing on mRNA transcripts. Additionally, BoNT/A injections have become the most popular cosmetic procedure worldwide, used to reduce wrinkles with effects lasting several months and impacting over 7 million people annually (18). Despite these advancements, neither basic research studies nor investigations into cosmetic applications have elucidated the downstream processes triggered by BoNT intoxication or the molecular mechanisms supporting neuronal survival. To address this gap, we aimed to elucidate the cellular responses to BoNT/A intoxication. Given recent insights into the regulatory roles of microRNAs (miRNAs) (19) we studied the involvement of small noncoding RNAs (sncRNAs) in these processes. Specifically, we profiled sncRNA transcripts in cultured human neuroblastoma cells following BoNT/A intoxication to identify miRNA, small-interfering RNAs, and the recently re-discovered transfer RNA fragments (tRFs) (20–22) that may contribute to postintoxication cellular responses.

tRFs are derived from the cleavage of both mature transfer RNA (tRNA) and tRNA precursors. Their biogenesis is highly regulated, depending on tissue, physiological state, and developmental stages of the cells or tissues in which they accumulate. This process reflects conserved and specific tRNA cleavage mechanisms, rather than random tRNA degradation (22, 23). tRFs typically range from 16 to 50 nucleotides (nt) in length and are endonucleolytic cleavage products of specific ribonucleases to generate shorter, functional fragments (24–26). Recent studies have revealed that tRFs play diverse roles across various nervous system cell types and organisms. Notably, tRFs targeting cholinergic transcripts have been

¹Department of Biotechnology, Israel Institute for Biological Research (IIBR), Ness Ziona 7410001, Israel; ²Department of Biological Chemistry, The Alexander Silberman Institute of Life Sciences, The Hebrew University of Jerusalem, Jerusalem 9190401, Israel; ³Obesity and Metabolism Laboratory, Institute for Drug Research, School of Pharmacy, Faculty of Medicine, The Hebrew University of Jerusalem, Jerusalem 9112001, Israel; ⁴The Edmond and Lily Safra Center for Brain Sciences, The Hebrew University of Jerusalem, Jerusalem 9190401, Israel; ⁵Department of Biochemistry and Molecular Genetics, IIBR, Ness Ziona 7410001, Israel; ⁶Department of Infectious Diseases, IIBR, Ness Ziona 7410001, Israel

Corresponding Author: Joseph Tam. E-mail: yossi.tam@mail.huji.ac.il; Osnat Rosen. E-mail: osnatr@iibr.gov.il; and Hermona Soreq. E-mail: hermona.soreq@mail.huji.ac.il

Received: 13 February 2025. Revised: 18 March 2025. Accepted: 25 April 2025.

Published online: 20 May 2025.





identified to predominantly originate from the mitochondrial genome (21) and exhibit a decline in abundance with age (23).

Multiple nucleases mediate the cleavage of tRNA and tRNA precursors to generate tRFs (27, 28). Importantly, tRFs can originate from either the nuclear or mitochondrial genome (29), and their functional roles are diverse. They may regulate protein translation in a manner akin to miRNAs (30) silence genes through base pairing with target mRNAs (20, 22, 31), or interact with RNA-binding proteins (32). The cleavage of tRNA molecules produces tRFs that can mediate neuroprotective effects by interacting with specific mRNA targets (33, 34). However, the potential role of tRFs in supporting the survival of human-originated neurons under botulinum intoxication, as well as the underlying mechanisms involved, remained unknown.

The immediate stress-induced accumulation of specific subtypes of tRFs facilitates the intracellular formation of stress granules, where these fragments localize to protect cells from acute stress (35). However, the processes occurring after the acute exposure phase remain poorly understood. In this respect, neuronal death in numerous neurodegenerative and neurological disorders has recently been linked to ferroptosis, a nonapoptotic cell death mechanism characterized by increased membrane lipid peroxidation, accumulation of lipid peroxides, and an inadequate capacity to counteract these processes (36–38). Neurons, being enriched in phospholipids containing polyunsaturated fatty acids (PUFAs) and iron (39, 40), rely on protective mechanisms to prevent lipid peroxidation under normal conditions. Interestingly, BoNT/A has been shown to alleviate cartilage degradation and inhibit osteoarthritis progression by preventing ferroptosis in chondrocytes (41). However, under pathological conditions, these defense mechanisms are compromised, promoting the recently identified ferroptosis cell death pathway (42). Despite this, the role of BoNT/A in modulating neuronal ferroptosis remains largely unexplored.

To study the molecular mechanisms underlying botulinum intoxication in neurons, we utilized the human-derived LAN5 neuroblastoma cell line (21). Small RNA profiling of BoNT/A-intoxicated LAN5 cells revealed profound changes in the neuronal transcripts landscape, suggesting a link between these changes and the mechanisms by which cholinergic neurotransmission is blocked while neuronal survival is maintained. Unexpectedly, our analysis uncovered a previously unrecognized accumulation of tRFs that initiate multiple protective pathways to both counteract neuronal death and inhibit ferroptosis. Furthermore, we identified a BoNT/A-induced accumulation of a repetitive tRNA-derived motif among the elevated postintoxication tRFs, which together appear to ensure the survival of intoxicated neurons by blocking ferroptosis. Deciphering these simultaneous protective pathways offers valuable insights into the mechanisms of BoNT/A-induced neuronal survival and may pave the way for novel BoNT/A-based therapeutic applications.

Results

Neuronal Survival Under BoNT/A Intoxication Involves Massive Transcriptomic Changes

The lethal dose of BoNT/A per person is estimated to range between 0.03 and 1 μ g depending on the route of administration (5). To explore the cellular response to BoNT/A intoxication, LAN5 human neuroblastoma cells were exposed to a potentially lethal dose of BoNT/A (10,000 MsLD₅₀/mL, equivalent to ~50 ng; Figure 1A), a concentration significantly higher than doses used in cosmetics applications (18). ELISA-based quantification of cleaved-SNAP25 levels (43) was used to establish a time-course assay, enabling the assessment of BoNT/A effects on LAN5 cells (Figure 1B). A dose–response curve spanning a wide range of BoNT/A concentrations was generated, yielding an EC₅₀ of approximately 4000 MsLD₅₀/mL (~120 pM toxin concentration) and a detection limit of 2–3 pM BoNT/A (Figure 1C).

An *in vitro* cell-based assay demonstrated neuronal survival following BoNT/A intoxication (13) (Figure 1D), providing a platform to explore molecular mechanisms regulating survival under such conditions. Long-read RNA sequencing (RNA-seq) of BoNT/A-intoxicated LAN5 cells identified differentially expressed (DE) transcriptomic changes, with 217 transcripts significantly downregulated and 135 transcripts upregulated

under BoNT/A exposure (Figure 1E and F and Supplementary Table S1), using a false discovery rate (FDR) of 0.05. Gene Ontology (GO) enrichment analysis of the downregulated transcripts revealed significant enrichment in biological processes such as *tRNA aminoacylation for protein translation* (Figure 1G). These findings suggested an altered repertoire in intoxicated cells of noncoding tRNAs, critical for protein synthesis and involved in diverse cellular processes and regulatory pathways.

BoNT/A-intoxicated LAN5 Cells Display Massive tRFs Accumulation

Small RNA-seq of total RNA from BoNT/A-intoxicated LAN5 cells and non-treated (NT) cells (Figure 2A, >12 million single reads per sample) was analyzed using miRExpress 2.1.4 (44) for miRNA levels and the MINTmap pipeline (45) with default parameters for tRF levels (using only reads mapping exclusively to the tRNA space). This analysis showed modest changes in miRNA levels (Figure 2B and Supplementary Table S2), which contrasted with massive increases and decreases in tRFs levels of both nuclear and mitochondrial genome origins (Figure 2C and D and Supplementary Table S3). Specifically, only 2 DE miRNAs were identified, whereas 335 DE tRFs were detected, with 63% upregulated under BoNT/A exposure. Among these, tRF-5' LysTTT (also known as tDR-1:31-Lys-TTT-3-M2 or tRF-31-P554PW3FJHPB) emerged as the most significantly elevated tRF in BoNT/A-intoxicated LAN5 cells (Figure 2E) compared to BoNT/E and TeNT toxin (Supplementary Figure S2). Classifying the DE tRFs by fragment type (Figure 2C and F) revealed that 189 of the 335 DE tRFs were internal tRFs, with 38 (all upregulated) originating from lysine tRNA and 51 from glutamate tRNA (most of them upregulated) (Figure 2G). Subdividing the DE tRFs by length showed that all of the upregulated tRFs were relatively long (25 nt and above), whereas the downregulated tRFs were short (less than 25 nt) and therefore more likely to function like miRNAs (Figure 2H). Together, these findings indicate a nonarbitrary fragment generation of regulatory sncRNAs during BoNT/A intoxication. Furthermore, the massive tRNA fragmentation observed likely corresponds to cell viability, as tRFs are known to be regulated under cell proliferation and are necessary for ensuring cell survival (46). To examine whether the cleavage we observed under BoNT/A exposure is unique to this condition or is shared by other types of stress, we utilized the GSE113751 dataset (47) of wildtype HEK293T cells under amino acid starvation (either Arginine (Arg) or Leucine (Leu)) or under no treatment for 3 or 6 h ($n = 12$, see *Materials and Methods*). Out of the 20,274 tRFs that were expressed in these cells, only 134 tRFs were shared with the 1654 tRFs found in the BoNT DE analysis. Moreover, none of those was significantly DE under amino acid starvation. Further, when comparing the log (FoldChange) of these 134 tRFs under BoNT/A intoxication and under amino acid starvation, only 14 showed the same trend of change (namely, over 1 or under –1 log (FoldChange) in both cases). The rest of the tRFs were either changed in one case only, or altered in opposite directions under the two stressors (Supplementary Figure S1). Thus, we show that the tRFs whose levels are changed under BoNT exposure reflect a “BoNT/A specific” signature.

BoNT/A-exposed LAN5 Cells and Rat Submandibular Glands Undergo Correlated Intoxication-induced tRFs Changes

To evaluate the relevance of our cell culture findings to *in-vivo* intoxication, we analyzed the small-read RNA-seq dataset from the submandibular glands of BoNT/A-injected rats versus control animals [GSE 141815 (48)], using the human MINTmap pipeline. This dataset revealed three DE tRFs out of the total of 92 detected tRFs (Figure 3A and Supplementary Table S4) ($P < 0.05$). Two of those (66%) corresponded to DE tRFs from BoNT/A-intoxicated human-originated LAN5 neurons (Figure 3B). Subdividing the entire tRFs repertoire based on the originating amino acid type families showed that most tRFs originated from lysine, glutamate, or histidine tRNAs ($\text{Log}_2\text{FC} > 1$). Furthermore, of the 52 total upregulated tRFs (DE and non-DE) in the BoNT/A-exposed rat dataset, 14 tRFs (27%) corresponded to DE tRFs from BoNT/A-intoxicated LAN5 neurons (Figure 3C). Specifically, among the 17 and 18 tRFs originating from lysine and glutamate tRNAs in BoNT/A-exposed rat glands (all nuclear-genome-originated), eight tRFs corresponded to lysine (47%) and 10 to glutamate (55%) DE tRFs identified in BoNT/A-intoxicated LAN5 cells (Figure 3D and E). Therefore, similarities between the DE tRFs identified in BoNT/A-exposed LAN5 cells were identical to tRFs with altered levels in poisoned

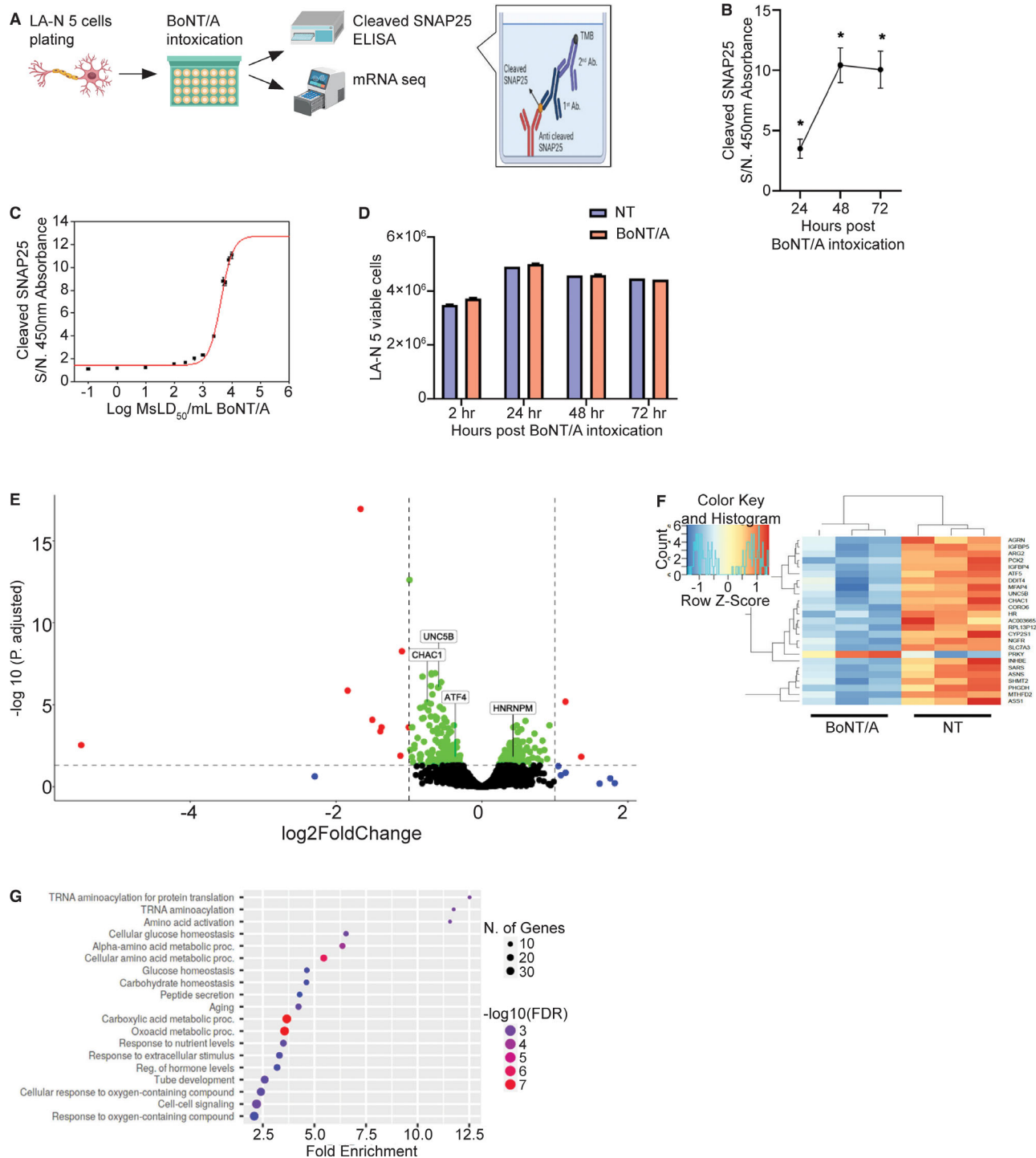


Figure 1. Assessing BoNT/A potency and molecular characterization of intoxicated LAN5 neuroblastoma cells. (A) Experimental setup: LAN5 cells (2×10^6 cells/well) were intoxicated with 10,000 MsLD₅₀/mL BoNT/A. Cleavage of SNAP25 was assessed using a specific sandwich ELISA assay. Long RNA-seq was performed for mRNA and lncRNA profiling. (B) Time-dependent signal-to-noise ratio (S/N) of cell lysates during BoNT/A incubation. S/N was calculated as the absorbance of BoNT/A-exposed cells divided by the absorbance of nontreated (NT) cells for all samples (duplicates). Data represent $N = 3$ biological replicates, analyzed by one-way ANOVA ($*P < 0.05$). (C) Dose-response curve for LAN5 cells exposed to BoNT/A concentrations ranging from 0.1 to 10,000 MsLD₅₀/mL, showing S/N ratios of cell lysates. (D) Time-course viability assay comparing NT cells to those exposed to 10,000 MsLD₅₀/mL BoNT/A. Viability was assessed using Alamar Blue fluorescence intensity (Ex: 530 nm, Em: 580 nm) at 2, 24, 48, and 72 h postpoisoning. Fluorescence signals were normalized to cell counts across three technical replicates. (E) Volcano plot displaying DE transcripts from long RNA-seq at 48 h postintoxication with 10,000 MsLD₅₀/mL BoNT/A. Red and green dots represent DE genes (FDR < 0.05), while blue and black dots indicate non-DE genes (FDR > 0.05). Differential expression analysis was performed by using the DESeq2 tool and Wald statistical analysis. Data reflect three biological replicates per treatment. (F) Heat map of the top 25 DE transcripts identified, visualized after variance-stabilizing transformation. (G) GO enrichment analysis of DE biological processes. Shown are processes with a fold enrichment >1.5.

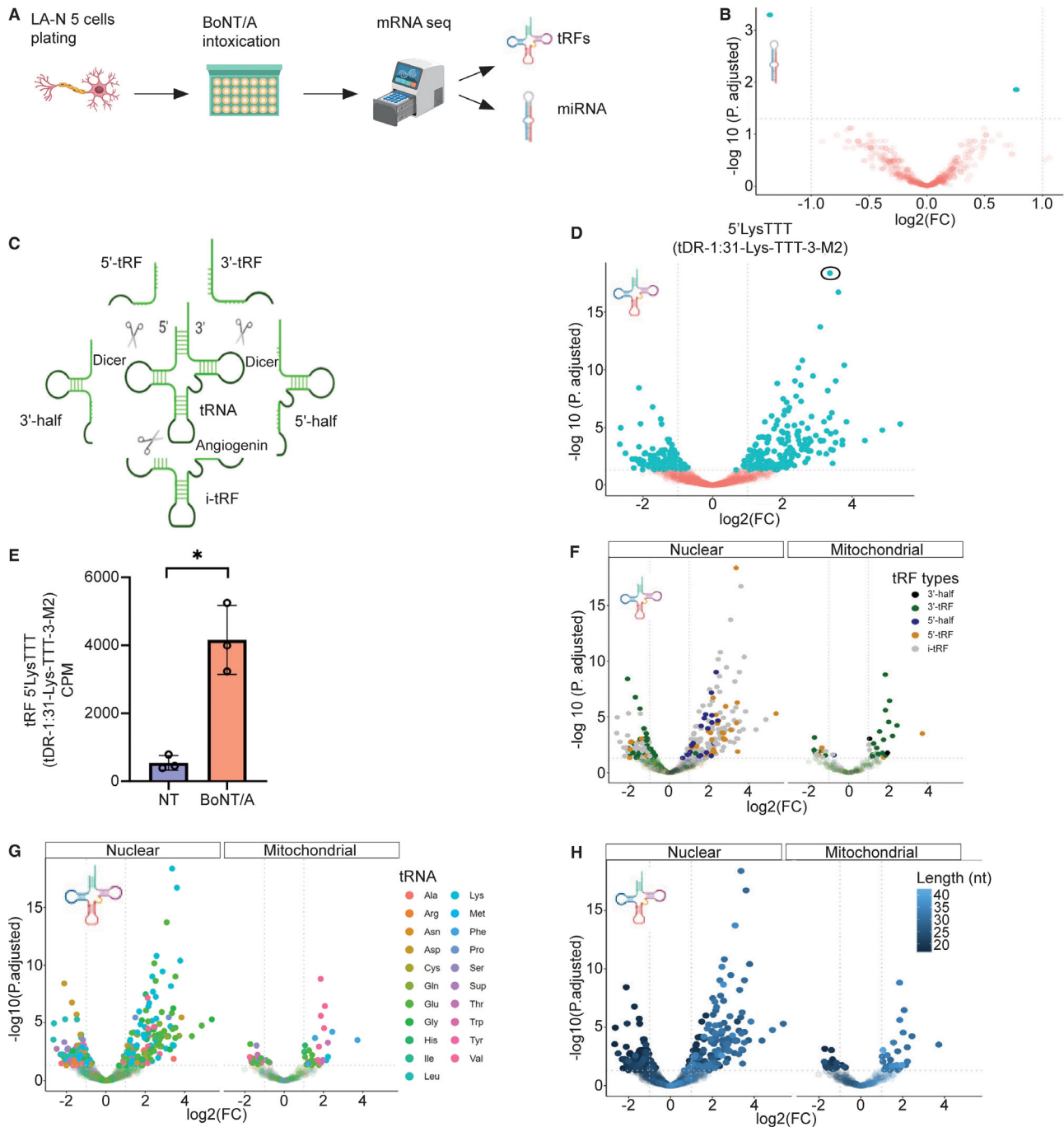


Figure 2. BoNT/A intoxication of LAN5 cells induces massive tRF changes. (A) Experimental design: 2×10^6 LAN5 cells/well were intoxicated by 10,000 MsLD₅₀/mL BoNT/A, and small RNA-seq profiles from these cells were compared to nontreated (NT) cells, revealing differences in miRNAs and tRFs. Volcano plots of DE transcripts (FDR < 0.05) were generated from three biological replicates per treatment. Differential expression analysis was performed using the EdgeR tool. (B) DE miRNAs. (C) Schematic representation of tRNA cleavage. (D) DE tRFs. (E) Levels of tRF-5'LysTTT were drastically elevated in BoNT/A-intoxicated LAN5 cells. Data represent $N = 3$ biological replicates; * $P < 0.05$. (F, G, H) Classification of DE tRFs by fragment type, corresponding amino acid, and length.

rat submandibular glands. These findings suggest an evolutionary conservation of the BoNT/A-intoxication response and its dose-dependent effects across mammalian tissues and neurons.

BoNT/A-upregulated Cholino-tRFs Predictably Target Numerous Cholinergic Transcripts

The observed changes in the transcriptomic landscapes of BoNT/A-exposed rat glands and human neuronal cells may reflect interrelated alterations in small RNA regulators, such as miRNAs (19) and tRFs (20). This

further predicted corresponding changes in the mRNA targets of those small RNAs whose levels were changed. To challenge this prediction and study the association between the analyzed small- and long-read RNA-seq datasets, we used the MR-microT DIANA prediction tool to identify predicted targets of the DE tRFs based on sequence motifs (49). This analysis was grounded in the conceptual framework that tRFs and miRNAs share the ability to interact complementarity with the 3'-untranslated region (UTR) of mRNA coding sequences (50). Using a combined prediction score that incorporates site conversion across species (51), we

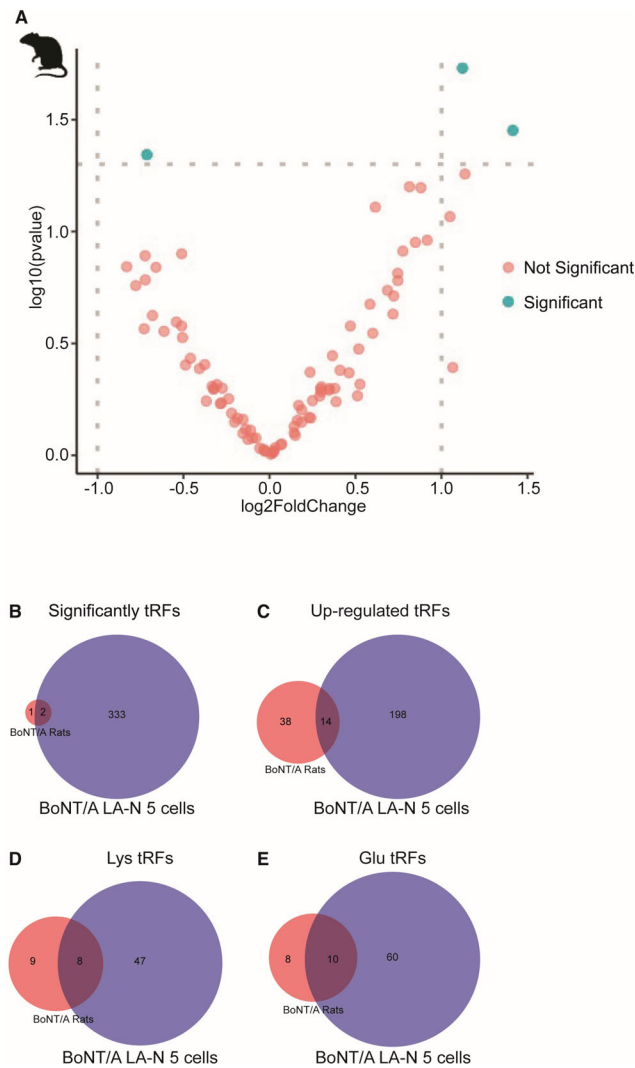


Figure 3. BoNT/A-intoxicated rat submandibular glands (GSE 141815) and human-derived LAN5 cells show closely related tRFs profiles. Small RNA-seq of rat submandibular glands following intoxication with six M₅LD₅₀/0.1 mL BoNT/A compared to a control group. $N = 4$ biological replicates. (A) Volcano plot depicting DE tRFs (P -value < 0.05), with four biological triplicates per treatment. Differential expression analysis was performed by using the DESeq2 tool and Wald statistical analysis. (B) Venn diagram illustrating the correlative significance of tRFs between LAN5 and rat datasets. (C) Venn diagram showing correlative upregulated tRFs between LAN5 cells and rat datasets. (D, E) Venn diagrams presenting correlative lysine tRFs levels between LAN5 cells and rat datasets and correlative glutamate tRFs levels between LAN5 cells and rat datasets.

extracted targets with a score below 0.8 for reliability (Figure 4A). Given that BoNT/A acts on cholinergic neurons forming cholinergic synapses at the NMJ, we further examined the potential of tRFs and miRNAs as regulators of synaptically expressed cholinergic genes. We defined “Cholino-tRFs” and “Cholino-miRs” as tRFs or miRNAs predicted to target either one core cholinergic gene [responsible for acetylcholine synthesis or breakdown, based on a cholinergic gene list acquired from (52)] or at least five genes associated with cholinergic activity. Sequence complementarity predictions formed the basis of this analysis (see *Materials and Methods*). Using this approach, our cell culture-derived small RNA-seq dataset included 11 DE Cholino-tRFs (Figure 4B and Supplementary Table S5) but no DE Cholino-miRs (Figure 4C). Among these, nine Cholino-tRFs were upregulated, while two were downregulated, all nuclear-originated, with 36% derived from glutamate tRNA fragments. These findings suggested

that Cholino-tRFs, rather than Cholino-miRs, may impact the cholinergic balance in BoNT/A-intoxicated neurons by regulating the expression of cholinergic genes.

Further analysis of the top 14 upregulated and 5 downregulated DE tRFs (originating from both mitochondrial and nuclear genomes) identified biological processes linked to their predicted target genes (Figure 4D and E). Processes such as “Neurogenesis,” “Generation of neurons,” and “Nervous system development” were enriched among the predicted targets of both upregulated and downregulated tRFs. These findings highlight the significant role of tRFs, compared to miRNAs, in modulating the neuronal response to BoNT/A exposure.

5’LysTTT tRFs Inhibit Ferroptosis in BoNT/A-intoxicated LAN5 Cells

5’LysTTT tRFs are known for their role in responding to stress by delaying cell death (53). Ferroptosis, a regulated nonapoptotic cell death mechanism dependent on iron and characterized by peroxidation of membrane lipids, is modifiable by cellular pathway modulation (54). This process involves the accumulation of lipid reactive oxygen species (ROS) or lipid peroxides derived from PUFAs, including arachidonic acid (AA), which serve as inducers of ferroptosis (55) (Figure 5A). BoNT/A intoxication triggered an endoplasmic reticulum (ER)-stress response that involves glutathione (GSH)-specific gamma-glutamylcyclotransferase 1 (*CHAC1*) (56) a regulator of ferroptosis that functions via GSH depletion (57). In BoNT/A-intoxicated LAN5 cells, we observed an accumulation of AA (Figure 5B), alongside other fatty acids (Figure 5C). This accumulation might stem from BoNT/A’s inhibition of AA release, previously reported in neurons (58). Correspondingly, we found increased levels of fluorescent ROS compounds (Figure 5D), indicating oxidative stress. However, we also found reduced transcription of cystine transporter solute carrier family 7 member 11 (*SLC7A11*) (Figure 5E), a cystine transporter critical for ferroptosis balancing as well as reduced transcription of Arginase 2 (*ARG2*) in both the long RNA-seq (Supplementary Table S1) and qRT-PCR data (Supplementary Figure S3), recent studies which have elucidated the role of *ARG2* as a key regulator in ferroptosis. Correspondingly, knockdown of *ARG2* increases lipid peroxidation, a hallmark of ferroptosis (59). Ferroptosis is governed by a complex network of genes and pathways, key regulators found in BoNT/A-intoxicated LAN5 long RNA-seq data that include those involved in iron metabolism (*FTH1*, *TFRC*, *TSC1*, *TSC2*, *EIF4EBP1*; Supplementary Table S1), lipid metabolism (*DGAT1*, *ACADVL*, *CPT1B*; Supplementary Table S1), antioxidant defense (*GCH1*; Supplementary Table S1) and metabolic enzymes (*PHGDH*, *SHMT2*, *MTHFD2*; Supplementary Table S1) which support NADPH production for GSH recycling, all regulating ferroptosis sensitivity (60, 61). Despite these changes, no ferroptosis was observed, potentially due to compensatory mechanisms. Supporting this prediction, long RNA-seq (Figure 1E) and qRT-PCR data (Figure 5F–H) revealed suppressed ferroptosis-related transcripts, including *CHAC1*, and those declined transcripts were exclusively decreased under BoNT/A intoxication, compared to BoNT/E or Tetanus toxin (Figure 5H).

Notably, *CHAC1* reduction may lead to GSH elevation (Figure 5I) and glutathione peroxidase 4 (*GPX4*) upregulation (Figure 5J), a potent ferroptosis antagonist (57). Using the tRFtarget 2.0 algorithm, we have further identified potential interactions between 5’LysTTT tRF and the 3’UTR of *CHAC1* mRNA (Figure 7K), indicating that tRF-5’LysTTT may exert a miR-like function to silence the *CHAC1* mRNA transcript. Experimental validation through a dual-luciferase reporter assay (62) showed a 20% reduction in Firefly/*Renilla* luciferase activity when 5’LysTTT mimic was cotransfected, confirming its miR-like function in silencing *CHAC1* mRNA (Figure 5L). Together, these findings highlight the role of 5’LysTTT tRFs in suppressing ferroptosis by targeting *CHAC1* and regulating neuronal ferroptosis-related genes, including *ATF4*, *DDIT3*, *CHAC1*, and *SLC7A11*. Furthermore, *CHAC1* transcript levels were not changed under overexpression of 5’LysTTT in LAN5 cells compared to control, indicating active contribution of BoNT/A to the reduction in *CHAC1* transcripts (Supplementary Figure S4). These molecular mechanisms likely contribute to neuronal survival after BoNT/A intoxication via ferroptosis inhibition and underscore the functional significance of tRFs in support of neuronal viability (Figure 5A).

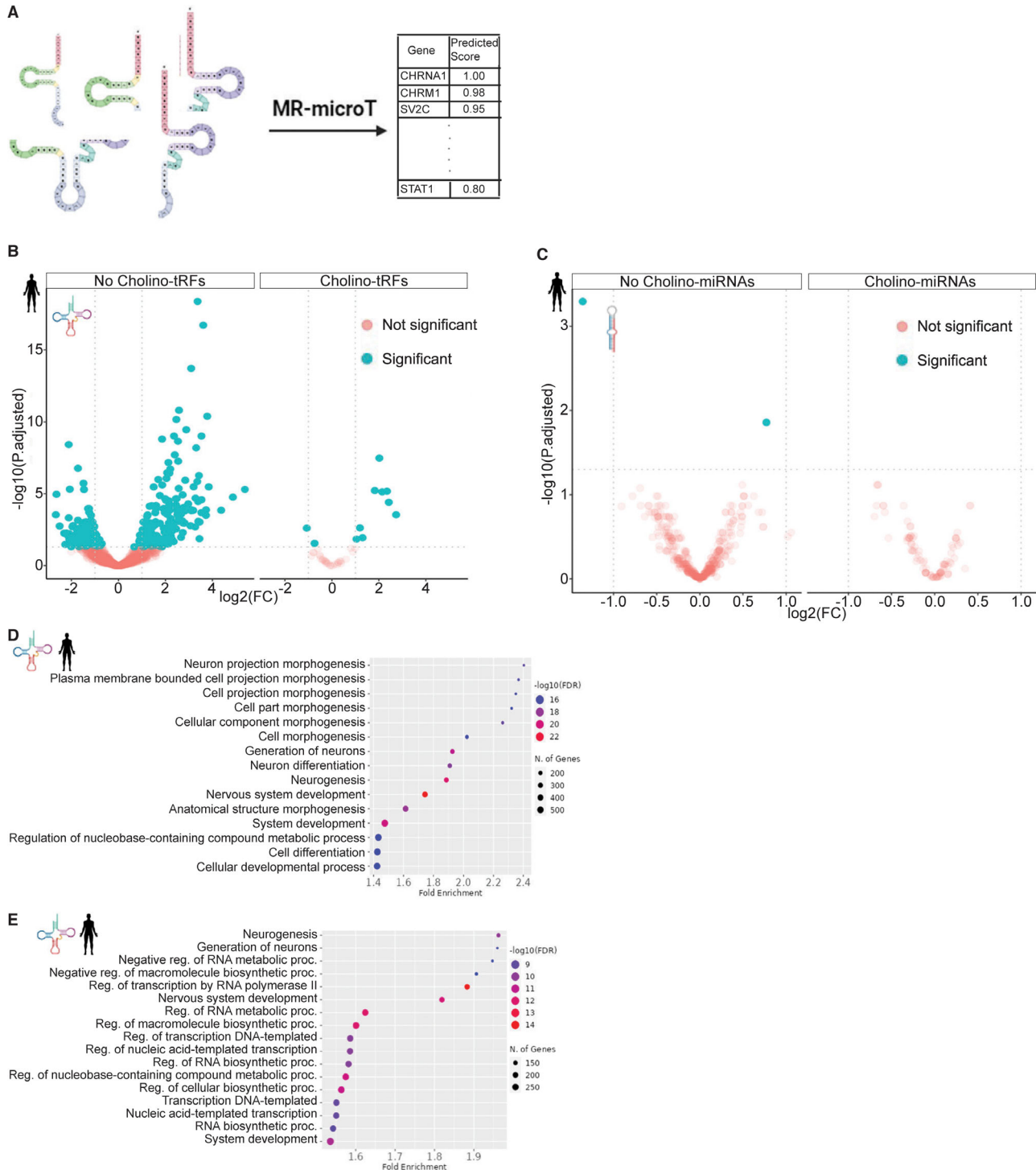


Figure 4. BoNT/A intoxication selectively upregulates nuclear genome-originated “Cholino-tRFs” affecting their predicted target genes. (A) A scheme representation of the predicted target gene analysis from small RNA-seq profiling of miRNAs and tRFs. LAN5 cells (2×10^6 cells/well) were intoxicated for 48 h by 10,000 MsLD₅₀/mL BoNT/A and compared to nontreated (NT) cells. DE transcriptomes (FDR < 0.05) were identified using three biological triplicates per treatment. (B) Proportion of DE tRFs and the fraction attributed to “Cholino-tRFs.” (C) Proportion of DE miRNAs and the fraction attributed to “Cholino-miRNAs.” (D) GO enrichment analysis of the top biological processes associated with the 14 most enriched upregulated DE tRFs (originating from mitochondrial and nuclear genomes). Analysis was conducted using www.ShinyGO.com with a fold enrichment cutoff >1.4. (E) GO enrichment analysis of the top biological processes associated with the five most enriched downregulated DE tRFs (originating from mitochondrial and nuclear genomes). Analysis was conducted using www.ShinyGO.com with a fold enrichment cutoff >1.5.

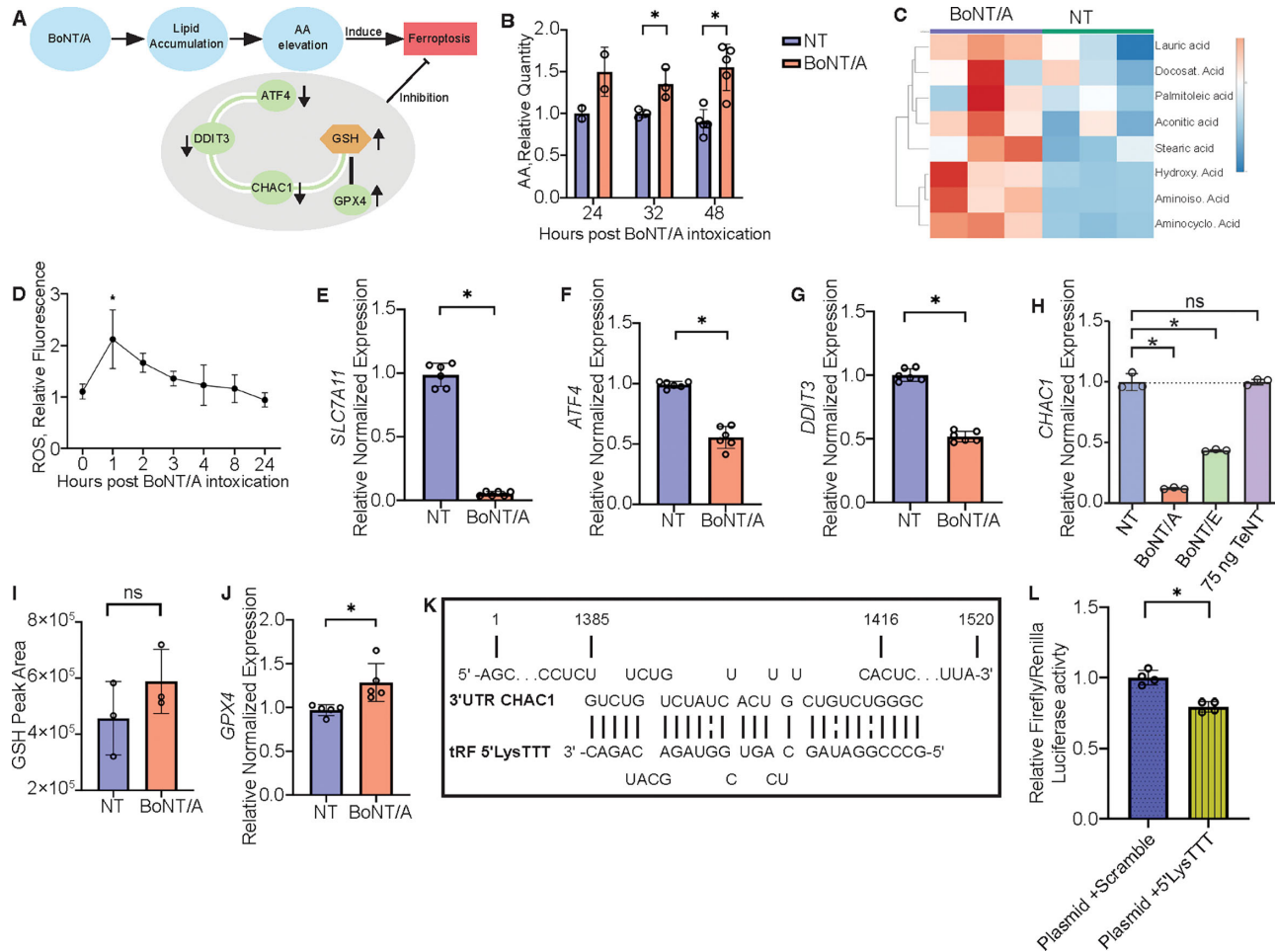


Figure 5. Declined ferroptosis-hub genes may support neuronal viability under BoNT/A intoxication. (A) Proposed mechanism by which ferroptosis is regulated after BoNT/A intoxication to maintain neuronal viability. (B) Arachidonic acid (AA) levels were measured under BoNT/A intoxication. AA was extracted from cells exposed to 10,000 MsLD₅₀/mL BoNT/A over 24–48 h and analyzed using LC-MS/MS. Levels were normalized to nontreated (NT) control cells. (C) Heat map of peak areas from fatty acids, analyzed by semitargeted metabolomics profiling. Polar extracts from BoNT/A-intoxicated LAN5 cells (10,000 MsLD₅₀/mL) were compared to NT samples and normalized to protein concentration. *N* = 3 biological replicates. (D) Relative ROS levels measured in BoNT/A-intoxicated cells (10,000 MsLD₅₀/mL) over 0–24 h. ROS were fluorescently detected, and data presented as mean ± SE. *N* = 3 biological replicates. (E) qPCR analysis of the *SLC7A11* transcript in LAN5 cells exposed to 10,000 MsLD₅₀/mL BoNT/A for 48 h. *GAPDH* served as a housekeeping gene. *N* = 6 biological replicates. **P* < 0.05. (F, G) qPCR of ferroptosis-related transcripts (*ATF4*, *DDIT3*) in LAN5 cells exposed to 10,000 MsLD₅₀/mL after 48 h of BoNT/A intoxication compared to NT cells. *GAPDH* served as a housekeeping gene. *N* = 6 biological replicates. **P* < 0.05. (H) qPCR of the *CHAC1* transcript in LAN5 cells exposed to 10,000 MsLD₅₀/mL after 48 h of BoNT/A/E and 75 ng TeNT intoxication compared to NT cells. *GAPDH* served as a housekeeping gene. *N* = 3 biological replicates. **P* < 0.05. (I) Glutathione (GSH) levels were analyzed using semitargeted metabolomics profiling of polar extracts from BoNT/A-intoxicated cells (10,000 MsLD₅₀/mL). Data normalized to protein concentrations. *N* = 3 biological replicates. (J) qPCR of *GPX4* transcripts in LAN5 cells exposed to 10,000 MsLD₅₀/mL BoNT/A for 48 h. *GAPDH* served as a housekeeping gene. *N* = 5 biological replicates. **P* < 0.05. (K) Sequence alignment of tRF-5'LysTTT with the 3'UTR of *CHAC1* mRNA, predicted using the tRFtarget.net 2.0 algorithm, suggesting potential sense–antisense interactions. (L) Dual-luciferase reporter assay demonstrating interaction of tRF-5'LysTTT with the 3'UTR of *CHAC1* mRNA. Cotransfection of the 3'UTR of *CHAC1* (psiCHECK-2 plasmid) with tRF-5'LysTTT mimic resulted in a significant 20% reduction in Firefly/Renilla luciferase activity compared to a scrambled sequence. *N* = 4 biological replicates. **P* < 0.05.

BoNT/A Suppresses the Formation of 5'LysTTT-HNRNPM Protein Complex, Reflecting the Outcome of Ferroptosis

To further explore the role of the modulated tRFs in BoNT/A-intoxicated cells, we next examined whether the DE tRFs could reflect the sustained viability of these cells. The most significantly modulated tRF in BoNT/A-intoxicated cells was tRF-5'LysTTT (as shown in Figure 2D and E). Due to its length and sequence features, we hypothesized that 5'LysTTT could interact with RNA-binding proteins. To test this hypothesis, biotinylated 5'LysTTT tRF oligonucleotides were conjugated to streptavidin magnetic beads, exposed to lysates from BoNT/A-intoxicated LAN5 cells, and the proteins selectively bound to the 5'LysTTT were analyzed (Figure 6A). Proteomic analysis using tandem mass spectrometry identified several proteins interacting with the biotinylated 5'LysTTT (Figure 6B and Sup-

plementary Table S6), one of which was heterogeneous nuclear ribonucleoprotein M (*HNRNPM*). *HNRNPM* is a well-known RNA-binding protein that regulates alternative splicing (63) and plays a role in neuronal ferroptosis (64). In our proteomic profiling, *HNRNPM* was found to be significantly enriched in BoNT/A-intoxicated cell lysates, as reflected by 15 unique *HNRNPM*-derived peptide fragments (Supplementary Table S6). Correspondingly, the *HNRNPM* mRNA transcript was significantly upregulated in the mRNA sequencing (mRNA-seq) dataset from BoNT/A-exposed cells (Figure 1E and Supplementary Table S1), and this was confirmed experimentally by qRT-PCR (Figure 6C). However, contrasting the upregulation of *HNRNPM* at the mRNA level, protein analysis revealed significantly reduced levels of *HNRNPM* in BoNT/A-treated cell lysates (Figure 6D), while no such reduction was observed in BoNT/E-treated cells (BoNT/E

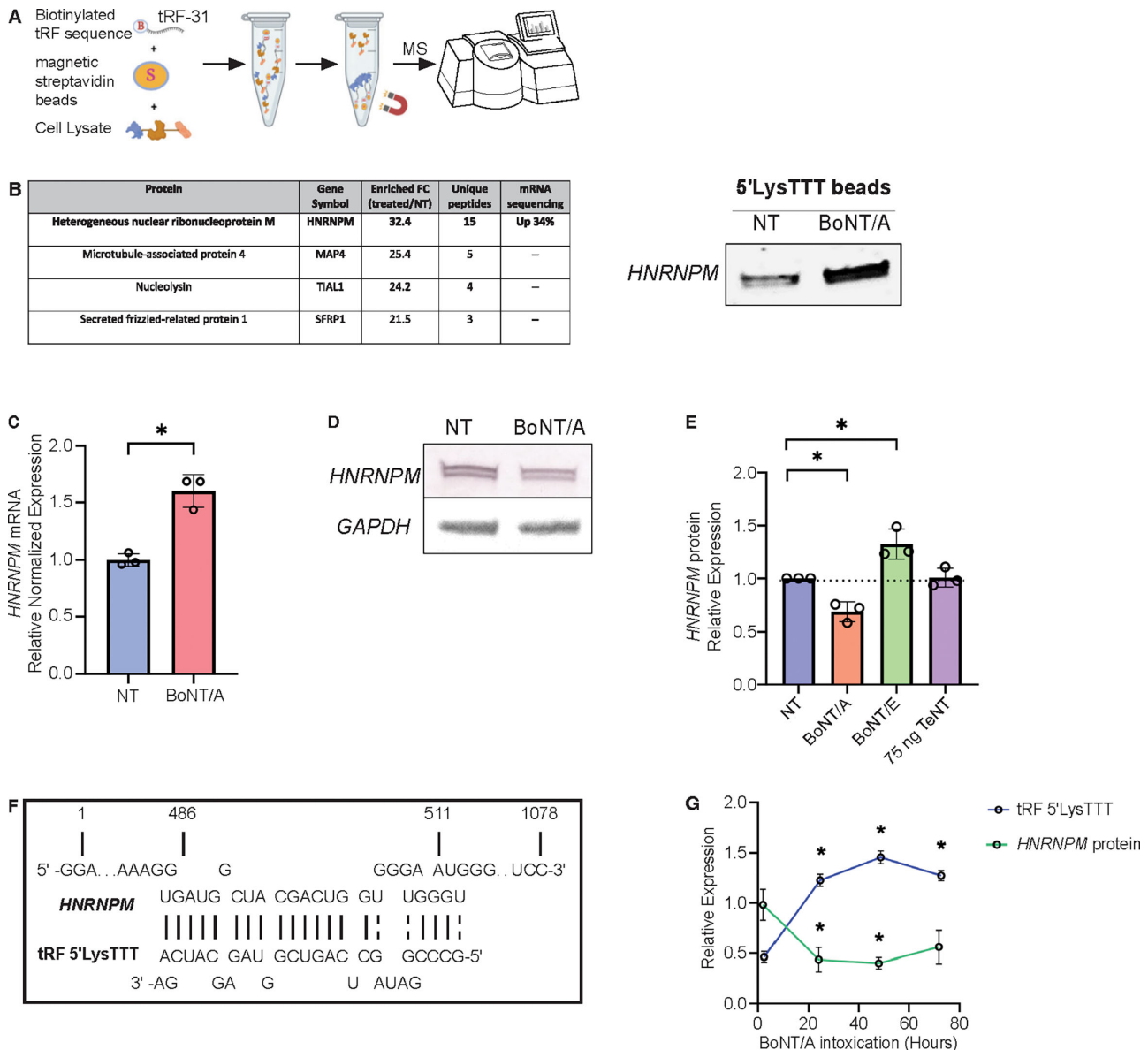


Figure 6. 5'LysTTT tRFs elevate *HNRNPM* regulation under BoNT/A intoxication. (A) A scheme illustrating the RNA pull-down assay conducted using biotinylated 31 nt 5'LysTTT tRF. (B) Proteins interacting with biotinylated 5'LysTTT tRF were analyzed by LC-MS/MS. The four highest scoring proteins that interacted with the tRF are shown, with high confidence peptides passing the 1% FDR threshold (left panel). The expression of *HNRNPM* was validated using immunoblot (right panel). *N* = 2 biological replicates. (C) qPCR analysis of *HNRNPM* mRNA expression was conducted on RNA extracts from BoNT/A-intoxicated LANS cells after 48 h of exposure to 10,000 MsLD₅₀/mL BoNT/A. Data normalized to *GAPDH*. *N* = 3 biological replicates. **P* < 0.05. (D) Representative immunoblots of the *HNRNPM* protein in cell lysates from BoNT/A-intoxicated LANS cells compared to nontreated (NT) cells, after 48 h of exposure to 10,000 MsLD₅₀/mL BoNT/A. The blots were normalized to *GAPDH*. *N* = 3 biological replicates. (E) Graphical analysis of *HNRNPM* relative expression in cell lysates (48 h, 10,000 MsLD₅₀/ml or equal) calculated *N* = 3 biological replicates. **P* < 0.05. (F) A sequence alignment of tRF-5'LysTTT (tDR-1:31-Lys-TTT-3-M2) and the *HNRNPM* mRNA was conducted using the tRFtarget.net 2.0 algorithm. The alignment showed potential sense-antisense interactions between this tRF and *HNRNPM* mRNA. (G) A time-course experiment analyzing the relative expression of *HNRNPM* by Western blot and quantifying 5'LysTTT tRF expression by qPCR after exposure to BoNT/A for 2–72 h (10,000 MsLD₅₀/mL). *N* = 3 biological replicates.

also cleaves SNAP25, but at a different position) or cells exposed to Tetanus neurotoxin (Figure 6E and Supplementary Figure S5). Using the tRFtarget 2.0 algorithm revealed predicted targeting by tRF-5'LysTTT of the *HNRNPM* transcript within its coding region (Figure 6F). This suggested that the elevation of 5'LysTTT and the parallel reduction in *HNRNPM* protein levels over time (Figure 6G) might indicate a direct impact of this snRNA on *HNRNPM* protein levels following BoNT/A intoxication. *HNRNPM* is functionally involved in a variety of cellular processes including alternative splicing (63), synaptic activity (64), immune response reg-

ulation (65), and the modulation of neuronal ferroptosis hub genes (66). Specifically, knockdown of *HNRNPM* has been shown to significantly enhance ferroptosis (67), highlighting its protective role. The inverse relationship between *HNRNPM* knockdown and ferroptosis aligns with the observed pattern of tRFs-5'LysTTT elevation and *HNRNPM* protein reduction, indicating a complex regulatory network balancing ferroptosis-related processes under BoNT/A intoxication. This reflects a delicate balance between upregulation and downregulation of ferroptosis pathways, ultimately influencing neuronal survival.



BoNT/A Upregulated tRFs Share an Amplified Sequence Motif

The intricate balance between regulators of ferroptosis following NoNT/A poisoning promoted a search into the controllers of this balanced response. In this respect, all tRNAs share significant portions of their sequences (20, 25). Furthermore, our findings of similar tRF responses to BoNT/A intoxication in human-derived cultured neurons and rat submandibular glands suggest an evolutionary conservation of this response. This raised the question of whether DE tRFs in humans and rodents share internal motifs (Figure 7A). Supporting this hypothesis, we identified a highly conserved 11-nt internal motif, "CCGATAGCTC" (Figure 7B), to be present in approximately 20% of the upregulated tRFs in BoNT/A-intoxicated human cells and rat tissues. This shared motif was also detected in the dataset from BoNT/A-intoxicated rat submandibular glands (Figure 3), with a minor variation at position 5 (adenine or cytosine in humans and only cytosine in rats, Figure 7B). Surprisingly, this motif was found in 14% of the tRFs in the rat gland dataset, despite the heterogeneous cell composition of these glands, which likely includes a lower abundance of neurons compared to human cell line cultures. This suggests that the observed elevation of motif-containing tRFs reflects the intoxication event rather than cell-type composition. Further analysis of sequences containing shared motifs in BoNT/A-intoxicated LAN5 cell datasets revealed a clear trend: longer motifs were progressively less represented among the total tRF numbers (Figure 7C). The 11-nt motif, derived from one of two lysine tRNAs (codons TTT and CTT), was detected in 20% of the upregulated tRFs but only 3% of the total tRFs in BoNT/A-intoxicated LAN5 cells (Figure 7D). This motif was absent in downregulated tRFs and exclusively originated from the 5' side of nuclear genome-derived tRNAs (Figure 7E). Moreover, this motif's composition significantly differed from that of the 7-nt motif previously identified in Parkinson's disease tissues and body fluids (68), suggesting its specificity to BoNT/A intoxication. Analysis using the MEME tool confirmed the overrepresentation of this motif in the analysed systems. This outcome predicted that RNA sequences carrying complementary regions to these motifs may be efficiently blocked during BoNT/A intoxication. Further, this also implies that the regulatory impact of this repetitive tRF motif (e.g., by targeting complementary mRNA transcripts) would be considerably more pronounced than that of single-copy tRF sequences.

Predicting that BoNT/A-induced tRFs may function similarly to miRNAs by interacting with complementary mRNA sequences to inhibit translation and promote degradation, (69) we searched for mRNAs with complementary sequences to the motif. Using the tRFtarget 2.0 algorithm, we identified the *UNC5B* transcript as a predicted target (Figure 7F). This mRNA, encoded by the cholinergic *UNC5B* gene, was first discovered in *Caenorhabditis elegans* flatworms exposed to anti-cholinesterases, resulting in movement impairments. (70) *UNC5B*, a netrin receptor, plays a critical role in axon extension during neural development (71). Therefore, we hypothesized that BoNT/A-induced motif-containing tRFs, acting in a miRNA-like capacity, (20) may silence *UNC5B* or reduce its expression, thereby impairing neurite extension. Indeed, *UNC5B* transcript levels were reduced by ~50% in BoNT/A-exposed cells (Figures 1E, 7G and Supplementary Table S1). This aligns with reports of BoNT/A-triggered arrest of nerve terminal sprouting, reflecting the toxin's effective duration. (72) Specifically, neuronal sprouting is crucial for restoring muscle contraction and re-establishing motor endplates by accelerating synaptic vesicle recycling (73). Remarkably, *UNC5B* also functions as a dependence receptor, promoting survival in the presence of its ligand, netrin-1. In the absence of netrin-1, *UNC5B* can induce apoptosis (74). However, mRNA-seq data from BoNT/A-intoxicated LAN5 cells showed no detectable netrin-1 (*NTN1*) transcripts (Figure 1E and Supplementary Table S1). This indicates that the downregulation of *UNC5B* in BoNT/A-intoxicated cells impairs cholinergic functions without compromising cell survival.

Together, these findings reveal the multifaceted roles for tRF-5'/LysTTT and the intoxication-induced repetitive motif in orchestrating the cosuppression of ferroptosis and cholinergic signaling while maintaining the survival of BoNT/A-intoxicated neurons.

Discussion

The impact of both whole-body BoNT/A intoxication and the locally injected toxin for cosmetic purposes (at far lower doses) may last 3–6 months in humans (75), and the protein changes involved have been well characterized (17, 76). However, the molecular regulators driving these changes and supporting neuronal survival under BoNT/A intoxication remain incompletely understood. To better understand the molecular processes underlying the response to BoNT/A, we profiled both long RNA (coding and long noncoding) and small noncoding RNAs (including miRNAs and tRFs) in BoNT/A-treated human-originated LAN5 cells, and sought relationships between these two datasets. Surprisingly, the short RNA profiles revealed a massive elevation of intoxication-induced tRFs and a contrasting minor miRNA response. Importantly, many of the DE tRFs contained sequences complementary to mRNAs expressed in these cells, and 20% of the intoxication-induced tRFs contained a repetitive 11-nt-long internal motif. Justifying this dual short and long RNA-seq approach, this comparison suggested a potentiated impact through short miRNA-like targeting by both miRNAs and tRFs of long cholinergic and pro-apoptotic transcripts, whose levels indeed declined in BoNT/A-intoxicated cells.

Unlike miRNAs, much is still unknown regarding the role of the recently re-discovered tRFs, their biogenesis, and functional mechanisms. Furthermore, while tRFs elevation under acute stress conditions has been studied by others and us in blood cells from postischemic stroke patients (20) and in degenerating brain neurons (21, 22) steatotic hepatocytes (77), and other human diseases, an in-depth understanding of the molecular mechanisms underlying specific cellular responses of tRFs to acute conditions is still in its infancy. Our findings of significant changes in tRFs profiles versus mild miRNA profile changes under BoNT/A intoxication may reflect the different impact and kinetics of miRNA changes compared to tRFs responses under acute stressors. Briefly, miRNA responses depend on transcription and transport to the site of their activity (in our case, the neuromuscular synapse), whereas tRFs changes are far more immediate, as they only require rapid cleavage by nucleases, including Angiogenin, Dicer, and Argonaut (31), from local tRNAs that are always present in all cells.

Exposing LAN5 human neuroblastoma cells to BoNT/A poisoning enabled us to reveal their BoNT/A sensitivity and EC₅₀ values, which closely correlated with findings from other cell lines and different BoNT/A intoxication protocols (43). Our long-read RNA-seq dataset from intoxicated human-originated neuroblastoma cells revealed numerous DE transcripts related to biological processes of "*tRNA aminoacylation*" which is altered by nucleases-driven breakdown of tRNAs (22, 25). This led us to explore the role of tRFs in BoNT/A intoxication, a recently rediscovered class of sncRNAs.

BoNT/A intoxication, whether accidental or therapeutic, leads to blockade of ACh release from NMJs. Accordingly, we identified DE transcripts that are reported to be NMJ-specific (78). Microarray studies in cell lines and human-induced pluripotent stem cells (hiPSC)-derived neurons under BoNT/A intoxication, as well as our current data, showed upregulation of mRNAs related to collagen deposition and apoptotic factors (79, 80). Based on this evidence, and on the surprising massive changes in BoNT/A-induced tRFs, our search into the molecular mechanisms driving these changes, while ensuring sustained viability of the affected cells, has focused on the unexpected upregulation and downregulation of specific tRFs in response to high leveled BoNT/A intoxication.

In addition to their remarkable toxicity, BoNTs may also positively impact neuronal outgrowth. The observed changes in tRFs profiles following BoNT/A intoxication are likely attributed to immediate posttranscriptional processes induced by neuronal intoxication. Correspondingly, the predicted target genes of those tRFs were enriched in processes such as "*neurogenesis*," "*generation of neurons*," and "*nervous system development*." For instance, neurons treated with BoNT/A are known to sprout new axonal branches (81). However, unlike rabies intoxication (82), this response enables long-term neuronal survival. Together, these findings indicate that BoNT/A intoxication induces a unique phenomenon that is distinct from other poisoning events or neurodegenerative states

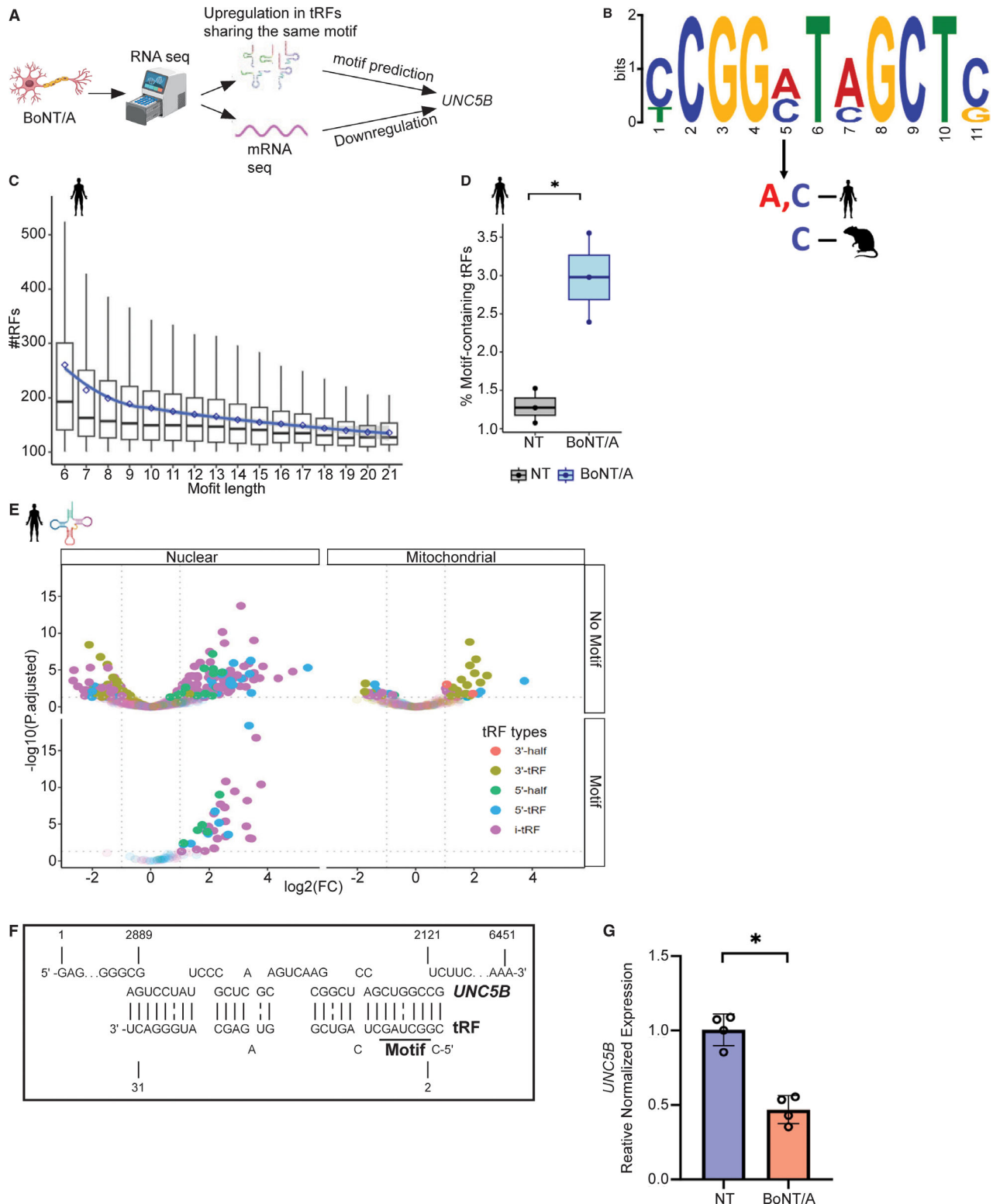


Figure 7. BoNT/A-intoxicated cells overproduce tRFs containing a common motif targeting the *UNC5B* gene. (A) Schematic representation of cholinergerg-targeted transcripts identified by both long and short RNA-seq. (B) Visualization of the CCGGATAGCTC motif using the MEME algorithm (<https://meme-suite.org/meme/>). (C) Box plots showing the number of different tRFs carrying motif sequences of 6–21 nucleotides that appeared in at least 100 tRFs in the BoNT/A-intoxicated LAN5 cells dataset. The graphs display median (box), mean (empty squares), and smoothed data. (D) Comparison of the percentage of tRFs from BoNT/A-intoxicated LAN5 cells (Treated) and nontreated (NT) cells carrying this motif, calculated from total tRFs in the BoNT/A-intoxicated LAN5 cells dataset. The graphs show median (box), mean (empty squares), and smoothed data. (E) Volcano plot of tRFs carrying this motif by fragment type in BoNT/A-intoxicated LAN5 cells. Shown are Volcano plots of DE transcriptomes (FDR < 0.05) with data from 3 biological replicates per treatment. Differential expression analysis was performed by using the EdgeR tool. (F) Sequence alignment of the CCGGATAGCTC motif and *UNC5B* mRNA using tRFtarget.net 2.0, showing potential sense-antisense interactions. (G) qPCR validation of *UNC5B* transcript levels. *GAPDH* served as a housekeeping gene (N = 4 biological replicates). *P < 0.05.



(21, 22). We conclude that tRFs may play a significant role in supporting neuronal survival following BoNT/A intoxication, but our current observations strongly suggest that they are unlikely to be involved in BoNT/A cosmetic uses due to the extremely low toxin concentrations employed.

Our study further established the predictable role for tRFs in forming complexes with RNA-binding proteins. In an *in vitro* pull-down assay, proteins interacting with biotinylated 5' LysTTT tRF from BoNT/A-cells lysate demonstrated affinity for HNRNPM, one of those RNA-binding proteins whose levels were elevated in BoNT/A-intoxicated neurons. Notably, HNRNP proteins play key roles in mRNA metabolism and are heavily involved in several neurodegenerative disorders (83). Further, *HNRNPM* suppression has been shown to promote ferroptosis in glioma cells (67). Hence, we postulate that the modulation of *HNRNPM* levels following BoNT/A intoxication may similarly arrest ferroptosis while supporting neuronal survival, processes which are inversely modulated by ferroptosis blockers.

Specific cells and structures of living organisms tend to carefully maintain homeostasis, suggesting that cells may deploy common mechanisms to respond to traumatic events. Instead of transcribing and transporting a miRNA to provide such response, cells can rapidly cleave tRNAs that harbor the required "seed" sequence (i.e., a sequence matching the 3'-UTR of a complementary miRNA target transcript) to generate multiple "miRNA-like" oligomers targeting the same transcripts. Given that tRNAs are highly conserved and abundant in all cell types, their cleavage can produce numerous copies sharing specific motif sequences. We have recently identified tRFs carrying a conserved 7-nt-long motif that accumulates in body fluids of Parkinson's disease patients in correlation with the initiation of disease emergence and inversely with their tremor events (68). Here, we report the accumulation of a longer, albeit less abundant 11-nt-long tRF motif derived from Lys tRNA, which can target and suppress the cholinergic *UNC5B* transcript, thus blocking cholinergic neurotransmission by the intoxicated neurons. Notably, this sequence emerges in approximately 20% of the postpoisoning tRFs, suggesting its substantial role in blocking cholinergic transmission in poisoned NMJs at large. Importantly, the tRFtarget.net prediction tool identified the observed internal repetitive motif sequence as capable of targeting several BoNT/A-intoxication downregulated mRNA transcripts, either within their coding regions or at their 3'UTR sites. This reflects a coordinated impact by groups of similar tRFs produced and acting together, generating "tRFs storms" that amplify their ability to silence specific transcript sets in response to BoNT/A intoxication.

The discovery of tRFs carrying repetitive motif sequences emerges from our current study as a reproducible event, reflecting the conserved sequences of mammalian tRNAs preserved in their breakdown products and corresponding to their length. Under random conditions, we calculated that approximately 1% of randomized upregulated and downregulated tRFs would carry shared sequence motifs. However, in the current dataset of BoNT/A-intoxicated LAN5 cells, an 11-nt-long shared motif appeared in 20% of the upregulated tRFs, suggesting a nonrandom event. The presence of this shared repetitive motif suggests that such sequences may vary depending on the stressor that triggered their nuclease-dependent emergence. The biological impact of their accumulation likely varies based on the stressor, the nuclease responsible for cleavage, the level of amplification under the specific conditions, and the mRNAs targeted by these motifs, which are characteristic of the biological process involved. At the observed concentration, BoNT/A intoxication triggers neuronal accumulation of tRFs carrying the internal "CCGATAGCTC" motif, which is complementary to the coding region of the cholinergic *UNC5B* mRNA, which recently was found to regulate neuronal ferroptosis (84). This was consistent with a reduction in *UNC5B* mRNA levels in intoxicated cells as well as with the predicted impact of BoNT/A intoxication which arrests cholinergic neurotransmission by the intoxicated neurons.

While the motif sequence identified in Parkinson's disease patients' blood is predicted to interact with and block the translation machinery (68), the motif sequence currently identified (present in approximately 20% of the BoNT/A-intoxication-elevated tRFs) may function as a "seed" domain, leveraging the tRFs' capacity to act like miRNA oligomers. In this respect, such repetitive sequences could be generated in relatively large quantities through tRNA cleavage, potentiating their impact on mRNAs

carrying complementary motifs. This amplification underscores the efficacy of tRNA-derived noncoding responses in mammalian cells and tissues.

Ferroptosis is a nonapoptotic cell death pathway characterized by the accumulation of lipid peroxides and mitochondrial dysfunction. Recent studies suggest that ferroptosis contributes to neurodegeneration in Parkinson's disease, Alzheimer's disease, and amyotrophic lateral sclerosis (85). In this context, RNA-seq profiling of BoNT/A-intoxicated neurons revealed a decline in transcripts involved in the ER stress pathway ATF4-CHAC1, which may regulate the threshold for ferroptosis-related death (86, 87). The observed coaccumulation of ferroptosis-related fatty acids and ROS in intoxicated cells from our model may provide a functional explanation for the molecular mechanisms underlying this process.

In addition to the miRNA-like functions of the intoxication-induced tRFs, we identified such interaction between the most potently BoNT/A-induced DE tRFs and *HNRNPM* mRNA, whose levels were significantly elevated postintoxication. Importantly, this tRF response efficiently suppressed HNRNPM protein levels, potentially promoting the ferroptosis pathway of programmed cell death (67). Further analysis of tRFs from BoNT/A-injected submandibular rat glands indicated that tRFs altered in LAN5 cells following BoNT/A exposure were also found *in vivo* in BoNT/A-exposed tissues. Classification of tRFs based on the amino acid encoded by their originating tRNA revealed that approximately 50% of the affected tRFs originated from lysine and glutamate tRNAs. Lysine tRNA fragmentation, previously reported to support the sustained viability of steatotic hepatocytes (77), appears to play a similar role across diverse cell types and tissues, as suggested by our findings.

Small- and long-read RNA-seq datasets revealed that a majority of DE tRFs were upregulated, correlating with a decline in many DE mRNA transcripts carrying complementary sequences to these tRFs. This finding suggests a miRNA-like function for some of the shorter tRFs (20), which may interact with mRNA transcripts carrying complementary sequence motifs (28). Notably, we identified a shared motif present in approximately 20% of BoNT/A-upregulated tRFs, which likely targets cholinergic genes by downregulating mRNA transcripts carrying tRF-complementary domains. This motif's significant occurrence among the upregulated tRFs population could amplify its regulatory impact, explaining the direct and substantial repression of *UNC5B* transcripts and the corresponding arrest of cholinergic neurotransmission that is known to appear under BoNT/A intoxication. Such repression might suppress cholinergic signaling, while the arrested ferroptosis preserves the viability of the intoxicated neurons.

The elevation of specific tRFs containing a repetitive motif sequence may stem from diverse biological origins: (1) BoNT/A intoxication may elevate specific tRNA levels, possibly due to translational arrest or a shortage of particular amino acids, leading to the breakdown of these tRNAs and the subsequent accumulation of their corresponding tRFs; (2) Increased levels or activity of specific nucleases could preferentially cleave certain tRNAs, resulting in the accumulation of selected tRFs; (3) Cellular mechanisms governing tRNA breakdown may be altered, promoting the survival of certain tRFs while degrading others; (4) A combination of the above processes could act together to produce the observed accumulation of tRFs carrying a repetitive motif. Interestingly, all of the motif-carrying tRFs whose levels were altered under BoNT/A intoxication in our human-originated cell line were derived from one of two nuclear genome-originated lysine tRNAs (codons TTT and CTT). This suggests that BoNT/A-induced accumulation of lysine-tRNAs may specifically contribute to the elevated levels of repetitive motif-containing tRFs observed in this study and thus determine its ultimate outcome.

Taken together, our findings suggest that the observed accumulation of AA may represent an immediate cellular response to BoNT/A poisoning, while the suppressed cell death reflects a longer-term outcome of this response. In this context, *CHAC1*, a downstream target of the ER stress pathway (88), plays a pivotal role in cell survival following BoNT/A-intoxicated LAN5 neurons, and may be a key factor selectively contributing to BoNT/A, but not to BoNT/E neuronal survival although both serotypes bind to the same receptor and cleave the same substrate. Correspondingly, the decline in *CHAC1* levels could actively promote the accumulation of GSH and



the upregulation of *GPX4*, both of which inhibit ferroptosis (89). Additionally, since tRF-5' LysTTT targets the 3' UTR of *CHAC1* transcripts, and given that *CHAC1* transcription is suppressed under BoNT/A intoxication, we hypothesize that the elevation of tRFs in response to BoNT/A exposure may serve as a trigger for both suppression of ferroptosis and sustained viability of the affected neurons.

New approaches to balance the duration of BoNT effects are poised to impact its clinical and cosmetic applications. Traditionally, clinical or cosmetic BoNT treatments last 3–4 months, but innovations reflecting the underlying molecular mechanisms might enable prolonged efficacy, lasting up to 6 months or more. In clinical settings, these extended-duration formulations could reduce treatment frequency for conditions like spasticity, migraines, and hyperhidrosis, improving patients' convenience and compliance while lowering health care costs (90). Similarly, in cosmetic applications, longer-lasting BoNT could provide sustained wrinkles reduction and muscle relaxation, appealing to patients seeking fewer appointments for maintenance (90). These advancements are likely to redefine treatment protocols across both therapeutic and aesthetic fields, offering more durable and efficient outcomes.

Our study involves certain limitations as well. First, the mechanisms observed here should be further challenged in other experimental models, as they may involve varying levels of BoNT/A intoxication due to differences in exposure time, toxin concentrations, and the use of purified neurotoxin, which could reflect its impact in other applications. Second, this study would benefit from validations using clinical samples from human BoNT/A intoxication cases, which were not available for this research.

In conclusion, our findings highlight distinct roles of sncRNAs, particularly poisoning-induced tRFs, in BoNT/A intoxication, acting as key drivers of the intoxication outcome and molecular pathways it activates, and ultimately supporting neuronal survival. The observed changes in tRFs induced by BoNT/A provide a plausible explanation for the sustained viability of intoxicated neurons in culture and poisoned rat glands, while also shedding light on the molecular mechanisms underlying the effects of poisoning over both short and long timelines. Enriching our knowledge of the central aspects of BoNT intoxication etiology may, therefore, pave the way for novel pharmaceutical strategies aimed at treating BoNT intoxication and/or enhancing its medical applications, ultimately improving human health and well-being.

Materials and Methods

Cell Culture, BoNT Intoxication, and Transfection

LAN5 neuroblastoma cells (DSMZ Catalog no. ACC-673), derived from a male donor, were cultured in RPMI-1640 medium (Biological Industries) supplemented with 10% FBS (Biological Industries), 1% L-Glutamine (200 mM, Biological Industries), and 1% penicillin-streptomycin-amphotericin solution (Biological Industries). The cells were maintained at 37°C in a humidified atmosphere containing 5% CO₂ and were passaged weekly using Trypsin-EDTA Solution A (0.25%) with EDTA (0.02%) (Biological Industries). For experiments, cells were plated in 12-well plates at a density of 2×10^6 cells/well in 1 mL of complete medium. *Clostridium botulinum* serotype A and E strains (A198 and E450, respectively) were sourced from the IIBR collection. Tetanus neurotoxin (TeNT) was procured from Sigma-Aldrich (Catalog no. T3694). Unless otherwise specified, LAN5 cells were intoxicated with 10,000 MsLD₅₀/mL (~300 pM) of BoNT/A/E for 48 h diluted in Neuro-Basal Medium (Biological Industries) supplemented with 2% FBS (Biological Industries), 1% L-Glutamine (200 mM, Biological Industries), and 1% penicillin-streptomycin-amphotericin solution (Biological Industries) and were compared to LAN5 cells cultured with Neuro-Basal Medium (Biological Industries) supplemented with 2% FBS (Biological Industries), 1% L-Glutamine (200 mM, Biological Industries), and 1% penicillin-streptomycin-amphotericin solution (Biological Industries) for 48 h without neurotoxin. 5' LysTTT transfection to LAN5 cells was as follows: 100 nM of tRF-5' LysTTT (GCC CGG AUA GCU CAG UCG GUA GAG CAU CAG A) and 100 nM of a control scrambled sequence (CGU UAA CCG CGC AUA AUA CGC GUA CGG GAG) were transfected to LAN5 using Lipofectamine3000 kit (L3000008, Invitrogen) according to the manufacturer's instructions.

Sandwich ELISA Assay for Cleaved SNAP25₁₉₇

Synthetic monoclonal antibodies specific to cleaved SNAP25₁₉₇ were generated as described previously (43). These antibodies (100 ng/well) were diluted in 50 mM bicarbonate buffer (pH 9.6) and used to coat polystyrene 96-well microtiter plates (Maxisorp, NUNC). Plates were incubated overnight at 4°C. The wells were washed three times with 300 μL/well of washing buffer (DDW, 0.9% NaCl, 0.05% Tween-20), followed by blocking with 250 μL/well TSTA buffer (DDW, 8.5% NaCl, 1 M Tris, 0.05% Tween-20, 2% BSA, pH 7.6) for 1 h at 37°C. For sample preparation, cells treated with or without neurotoxin were washed once with PBS and lysed in freshly prepared Triton X-100 lysis buffer (50 mM HEPES, 150 mM NaCl, 1.5 mM MgCl₂, 1 mM EGTA, 1% Triton X-100, and one EDTA-free protease inhibitor tablet). Lysates were centrifuged at 12,000 rpm for 5 min, and 50 μL of supernatant was added to the wells for 1 h incubation at 37°C. After washing three times, wells were incubated with polyclonal rabbit anti-SNAP25 antibodies (Catalog no. S9684, Sigma-Aldrich) diluted 1:5000 in TSTA buffer containing 1% normal mouse serum (NMS) and 1% normal human serum (NHS) for 1 h at 37°C. Following another wash, 50 μL/well of Horseradish peroxidase (HRP)-conjugated donkey anti-rabbit antibodies (Catalog no. 711-035-152, Jackson) diluted 1:1000 in TSTA buffer with 1% NMS and 1% NHS was added for 30 min at 37°C. The enzymatic reaction was visualized using 50 μL/well of KPL Sureblue (Catalog no. 5120-0081, Seracare) substrate for 10 min at room temperature. The reaction was stopped by adding 100 μL/well 0.5M H₂SO₄, and absorbance was measured at 450 nm. Lysates from neurotoxin-free cells served as controls in all assays. Signal-to-noise (S/N) ratios were calculated for each treatment.

Cell Viability

For calibration curves, 2 mL of 800,000 cells/mL were added to one well of a 24-well plate (COSTAR). A total of 1 mL of fresh medium was placed in the other five wells in the same row. Then, 1 mL of 800,000 cell/mL was moved to the adjacent well and cells were serially diluted across the entire row so that wells contained 800,000, 400,000, 200,000, 100,000, and 50,000 cells/mL. The last well in the row was left with 1 mL fresh medium as a negative control. 1 mL samples of counted cells were added to each well and supplemented with 100 μL Alamar blue (Catalog no. G8081, Promega). Plates were covered by aluminum foil for protection from light and incubated for 1 h at 37°C without CO₂. Then, plates were read in a M200 plate reader (TECAN, NEOTEC BIO), with excitation: 550 nm, emission: 580 nm filters. Remaining cell numbers were calculated based on the calibration curves.

Long-read mRNA-seq

Total RNA was extracted from LAN5 cells intoxicated with 10,000 MsLD₅₀/mL BoNT/A for 48 h and from nontreated LAN5 cells (NT) using the RNeasy Mini Kit (Catalog no. 74104, Qiagen) according to the manufacturer's instructions. RNA quantity and quality were assessed using Bioanalyzer (Cat# G2964AA, Agilent) with the RNA High Sensitivity Kit ScreenTape (Catalog no. 5067-5579, Agilent). RNA integrity numbers (RIN) were calculated, and samples with RIN value >8.0 were selected for sequencing at the Columbia Genome Center (NY, USA) and the Genomic Technologies Facility at the Hebrew University of Jerusalem, Israel. Libraries were generated from 1 μg of total RNA using the TruSeq RNA Library Preparation Kit (Catalog no. RS-122-2001, Illumina), and whole transcriptome sequencing (total RNA-seq) was performed using an Illumina HiSeq. Over 20 million single-end 100 nt reads per sample were generated. RTA (Illumina) for base calling and bcl2fastq2 (version 2.19) for converting BCL to fastq format coupled with adaptor trimming was performed. Pseudoalignment to a Kallisto index was created from transcriptomes (Human:GRCh38.p12) using Kallisto (0.44.0) (91). Normalization, visualization and differential transcript analyses were performed using the DESeq2 tool to test differential expression between two experimental groups from RNA-seq counts data, with significantly altered transcripts identified by calculating FDR < 0.05. GO enrichment analysis was conducted using the Gene Ontology Resource (<http://geneontology.org/>) as per the provided guidelines.

**Table 1.** Primers used in this study

Transcript	Forward Primer	Reverse Primer
<i>UNC5B</i>	GTCGGACACTGCCAACTATAC	CCGCCATTACACGTAGACGAT
5'Lys TTT	GCCCCGATAGCTCAGTCGGT	TTTTTTTTTCTGATGCTCT
<i>HNRNPM</i>	CTCTTAATGGACGCTGAAGGAAA	CGCTCAGACTATGCTTGTTTAGG
<i>SLC7A11</i>	GGTCCATTACCAGCTTTGTACG	GGTCCATTACCAGCTTTGTACG
<i>ATF4</i>	CCCTTCACCTTCTTACAACCTC	TGCCAGCTCTAACTAAAGGA
<i>DDIT3</i>	GAAACAGAGTGGTCATTCCC	CTGCTTGAGCCGTTTCTTCTC
<i>CHAC1</i>	GTGGTGACGCTCCTTGAAGA	GAAGGTGACCTCCTTGGTATCG
<i>GPX4</i>	GAGGCAAGACCGAAGTAAACTAC	CCGAAGTGGTTACACGGGAA
<i>GAPDH</i>	AGGGGTCTACATGGCAACTG	CGACCACTTTGTCAAGCTCA
3'UTR <i>CHAC1</i>	TCTACTCGAGGTGCTCATGTGGACATCAGG	TAAGCGCCGCTAAAGAGATAGTTTTATGGG

Small-read RNA-seq

Total RNA was extracted from LAN5 cells intoxicated with 10,000 M_sLD₅₀/mL BoNT/A for 48 h and from nontreated LAN5 cells (NT) using the miRNeasy Mini Kit (Catalog no. 1038703, Qiagen) according to manufacturer's instructions. RNA yields were quantified, and RNA quality was assessed using the Bioanalyzer (Catalog no. G2964AA, Agilent), with the RNA High Sensitivity Kit ScreenTape (Catalog no. 5067-5579, Agilent). RIN values were calculated and samples with RIN value >8.0 were sent to LC Sciences (Houston, USA) for small-read RNA-seq of a small RNA library generated from 1 µg of total RNA using the TruSeq Small RNA Sample Prep Kits (Catalog no. RS-200-0012, Illumina). Single-end sequencing of up to 50-nt-long reads was performed on an Illumina HiSeq 2500. Over 12 million single reads per sample were generated. FASTQ files were quality checked with FastQC (92) according to the pipeline recommended definitions, and then adaptors were removed using FLEXBAR (93) according to the pipeline instructions. Adaptor-less reads were aligned to miRs (miR-Base v21) using miRExpress 2.1.4 (44) with default parameters, and to tRFs using the MINTmap pipeline (45) with default parameters for tRF levels, and using only reads that mapped exclusively to the tRNA space. After the alignment, differential expression analysis of miRs and tRFs was conducted using EdgeR (94): Lowly expressed features were filtered with filterByExpr. Normalization factors were calculated with calcNormFactors, and dispersion estimates were obtained using estimateDisp. A generalized linear model was fitted (glmQLFit) and calculated, and differential expression was assessed using quasi-likelihood F-tests (glmLRT). Finally, results were extracted with topTags, applying false discovery rate (FDR) correction.

Analysis of the GSE113751 Dataset

To enable consistent and straight forward analysis, we analysed only HEK293T samples from the GSE113751 dataset, and only of wildtype background (i.e., noninfected cells or cells infected with an AAV that carries GFP alone). We regarded both Arg and Leu starvation as "stress" and the DE design matrix consisted of comparing stressed to control cells, accounting for starvation time, and noted if cells were transfected with a GFP-carrying AAV or not transfected at all. This analysis (alignment, normalization and differential expression analysis) was similar to the analysis for small-read RNA-seq (the previous section) (47).

Quantitative PCR and Gene Expression Assessment

Total cellular RNA was extracted from LAN5 cells intoxicated with 10,000 M_sLD₅₀/mL BoNT/A for 48 h and from nontreated LAN5 cells (NT) using the TRI reagent (Catalog no. T9424, Sigma-Aldrich) with either RNeasy (Catalog no. 74104, Qiagen) or miRNeasy Mini Kit (Catalog no. 1038703, Qiagen; for enrichment of small RNA fragments) according to manufacturer's instructions. Total RNA concentration was determined using the Qubit RNA HS Assay Kit (Catalog no. Q10211, Invitrogen). RNA was reverse-transcribed to cDNA using the Maxima First Strand cDNA Synthesis Kit (Catalog no. K1671, Thermo Fisher Scientific) which includes a DNase treatment step to eliminate genomic DNA, and diluted 1:10 in double-distilled water before preparing the quantitative PCR (qPCR)

plate. For tRF-5'LysTTT quantification, total RNA was reverse-transcribed using the qScript miRNA cDNA Synthesis Kit (Catalog no. 95107-025, QuantaBio). qPCR was performed in 96-well plates on the LightCycler 96 Instrument (Roche) using Universal SYBR Green Supermix (Catalog no. 1725150, Bio-Rad) with a final well volume of 15 µL. Glyceraldehyde-3-phosphate dehydrogenase (*GAPDH*) served as the housekeeping gene. Gene expression was calculated as $\Delta\Delta C_t$ values using the LightCycler 96 System Performance Data by Roche. Primer sequences are provided in Table 1.

RNA Pull-down Assay

Biotin-labeled tRF-5'LysTTT and a corresponding scrambled sequence were synthesized by IDT (Coralville, IA, USA). RNA pull-down from BoNT/A-intoxicated and NT cell lysates was performed using The Pierce Magnetic RNA-Protein Pull-Down Kit (Catalog no. 20164, Thermo Fisher Scientific) following the manufacturer's protocol, as described previously (22). tRF-5'LysTTT (GCC CGG AUA GCU CAG UCG GUA GAG CAU CAG A) and a control scrambled sequence (CGU UAA CCG CGC AUA AUA CGC GUA CGG GAG G) were designed with the two penultimate bases protected by 2'-O-methylation to prevent 3'-end degradation. Pull-down proteins were analyzed by mass spectrometry at the Smoler Proteomics Center, Technion, Israel.

Western Blot Analysis

SDS-PAGE was performed using NuPAGE 10% Bis-Tris gels (Catalog no. NP0301BOX, Invitrogen). Cell lysate samples, diluted in a Tris-Glycine SDS Sample Buffer, were subjected to transfer using the Nitrocellulose Western iBlot Gel Transfer Semi-dry system (Invitrogen). Membranes were blocked with 5% skim milk diluted in PBST (PBS containing 0.05% Tween-20) and incubated with monoclonal mouse anti-HNRNPM1-M4 (Catalog no. NB200-31455, Novus) primary antibody, followed by HRP-conjugated Donkey anti-Mouse (Catalog no. 715-035-152, Jackson) secondary antibody. Immunoreactive bands were visualized using the TMB Liquid Substrate System for Membranes (Catalog no. T0565, Sigma-Aldrich), detected with the FUJIFILM LAS-3000 imaging system, and analysed using ImageJ software.

AA Extraction and Measurement by LC-MS/MS

AA extraction, purification, and quantification were performed using stable isotope dilution liquid chromatography/tandem mass spectrometry (LC-MS/MS) as previously described (95). Briefly, AA from BoNT/A-intoxicated and NT cell lysates was precipitated using ice-cold acetone and 50 mM Tris buffer (pH 8.0). An ice-cold extraction buffer (1:1 MeOH/Tris Buffer) containing the internal standard [_d4-AEA] was added to the samples, followed by homogenization. The homogenates were extracted with ice-cold CHCl₃: MeOH (2:1, vol/vol), and the extraction was repeated with three washes of ice-cold chloroform. The samples were then dried under a nitrogen stream and reconstituted in MeOH. LC-MS/MS analysis was conducted on an AB Sciex (Framingham, MA, USA) QTRAP 6500 + mass spectrometer coupled with a Shimadzu (Kyoto, Japan) UHPLC system. Liquid chromatographic separation was



performed on a Kinetex 2.6 μm C18 (100 \times 2.1 mm) column (Phenomenex, Torrance, CA, USA) with the autosampler temperature set to 4°C, and the column maintained at 40°C throughout the analysis. Gradient elution was carried out using mobile phases of 0.1% formic acid in water (phase A) and 0.1% formic acid in acetonitrile (phase B). AA was detected in a positive ion mode using electron spray ionization and a multiple reaction monitoring (MRM) acquisition mode. AA levels were quantified against standard curves and normalized to total protein concentration in the samples. Relative AA quantities were compared between BoNT/A-exposed and untreated cells.

LC-MS Metabolomics Analysis

For fatty acids and GSH measurements, pellets from BoNT/A-intoxicated and NT cells were harvested with 400 μL of cold (-20°C) metabolite extraction solvent (MeOH:acetonitrile:water, 5:3:2) and kept on ice. Extracts were centrifuged at 18,000 $\times g$ for 15 min at 4°C, and the supernatants were collected into microcentrifuge tubes. These were re-centrifuged at 18,000 $\times g$ for 10 min at 4°C, then transferred to glass high-performance liquid chromatography (HPLC) vials and stored at -70°C . LC-MS metabolomic analysis was performed as described previously (96). Briefly, a Dionex Ultimate 3000 high-performance liquid chromatography (UPLC) system coupled to an Orbitrap Q-Exactive Mass Spectrometer (Thermo Fisher Scientific) was used with a resolution of 35,000 at 200 mass/charge ratio (m/z). Electrospray ionization and polarity switching mode enabled transport of both positive and negative ions across a mass range of 67 to 1000 m/z . The UPLC system utilized a ZIC-pHILIC column (SeQuant; 150 mm \times 2.1 mm, 5 μm ; Merck, Darmstadt, Germany) with a ZIC-pHILIC guard column (SeQuant; 20 mm \times 2.1 mm). A 5 μL sample of cell extract was injected, and the compounds were separated using a mobile phase gradient over 15 min, starting at 20% aqueous (20 mM ammonium carbonate, adjusted to pH 9.2 with 0.1% of 25% ammonium hydroxide) and 80% acetonitrile, then terminating with 20% acetonitrile. The flow rate was set to 0.2 mL/min and the column temperature to 45°C, with a total run time of 27 min. Metabolite analysis was performed with a mass accuracy of less than 5 ppm. Data acquisition was done using Thermo Xcalibur, followed by analysis in TraceFinder 4.1 (Thermo Fisher Scientific, Waltham, MA, USA). The exact mass and known retention time of singly charged ions were determined using an in-house MS library created by running commercial standards for all detected metabolites. The intensity of each identified metabolite was normalized to total protein concentration of each sample.

Measuring Oxidative Stress

Total cellular ROS levels in adherent cells were determined using 2',7'-dichlorodihydrofluorescein diacetate (DCFH-DA, Catalog no. D6883; Sigma-Aldrich) staining, as described previously (97). DCFH-DA is a widely used probe for total ROS detection, where it is taken up by cells and cleaved by cellular esterases, releasing DCFH. Oxidation of DCFH by ROS produces for 2'-7'-dichlorofluorescein (DCF), which emits green fluorescence upon excitation at 485 nm and emission at 530 nm. To assess ROS levels, 20 μM DCFH-DA was added to both BoNT/A-intoxicated and NT cells, which were incubated for 30 min under standard culture conditions, protected from light. After incubation, the medium was replaced with fresh medium, and DCF fluorescence was measured using a TECAN M200 plate reader (NEOTECH BIO). Relative fluorescence intensities were calculated by comparing the signals from BoNT/A-treated cells to untreated controls.

Construction of a psiCHECK-2 Plasmid Containing the 3'UTR of CHAC1 mRNA

Genomic DNA extracted from LAN5 neuroblastoma cells (DNeasy Blood & Tissue Kit, Catalog no. 69504, Qiagen) was used as the template for PCR amplification of the 3'UTR of the *CHAC1* gene (717 bp). Specific primers, including flanking regions for *PspXI* and *NotI* HF restriction enzymes (Table 1), were used for amplification. The amplified product was gel-purified using the QIAquick Gel Extraction Kit (Catalog no. 28704, Qiagen). The PCR product was then digested with *PspXI* and *NotI* HF restriction enzymes in rCutSmart buffer (10 U; New England Biolabs, Ipswich, MA) and purified using the QIAquick PCR Purification Kit, Cata-

log no. 28104, Qiagen). The psiCHECK-2 plasmid (1 μg ; Promega) was digested sequentially with *PspXI* and *NotI* HF in rCutSmart buffer (10 U; New England Biolabs, Ipswich, MA). The purified insert and vector were ligated with T4 ligase (200 U, 20 μL reaction, 1:3 vector/insert ratio; New England Biolabs). Transformation of ligated constructs into competent *Escherichia coli* cells following by PCR colony screening identified positive clones. The composition of the resulting psiCHECK-3'UTR *CHAC1* plasmid was confirmed by PCR.

Transfection and Dual-luciferase Assay of the psiCHECK-3'UTR CHAC1 Vector

HEK293 cells (1×10^5 cells/well) were seeded in a 24-well plate. After 24 h, the psiCHECK-3'UTR *CHAC1* vector was cotransfected with 100 nM of tRF-5'LysTTT or a corresponding scrambled sequence using Lipofectamine 3000 (Catalog no. L3000015, Invitrogen) according to the manufacturer's instructions. Following 48 h of incubation, the media were removed, and cells were lysed. Dual luciferase activity was measured using the Dual Luciferase Reporter Assay Kit (Catalog no. K1910, Promega).

Statistics

Data are presented as mean \pm SEM. Statistical differences between two groups were assessed using unpaired two-tailed Student's *t* test. For comparisons among multiple groups, one-way ANOVA followed by a one-sided Tukey test was used. All analyses were performed using GraphPad Prism v8 for Windows (San Diego, CA). A significance level of $P < 0.05$ was set for all comparisons.

Computational Tools

Repetitive sequence motifs in the characterized tRFs were identified using the MEME suite tool (<https://meme-suite.org/meme/index.html>) (98). For target prediction of these sequences, the tRFtarget.net 2.0 and MR-microT DIANA algorithms were employed (49, 99, 100).

Data Availability

The data that support the findings of this study are available upon request from the corresponding author: hermona.soreq@mail.huji.ac.il

Acknowledgments

We thank Dr. Adi Kedmi (IIBR) and Mrs. Edith Lupu (IIBR) for fruitful discussions. We also thank Mrs. Atara Uzan for graphical assistance.

Author Contributions

A.M., N.M., J.T., O.R. and H.S.: Conceptualization; A.M., J.T., O.R. and H.S.: Methodology; A.M. and O.R.: Investigation; A.M, N.M, S.V.T, O.I., L.H.: Formal Analysis; A.M., N.M.: Writing – Original Draft; J.T., D.S.G., O.R. and H.S.: Writing – Review & Editing; A.M., N.M., O.R., H.S.: Visualization; J.T., H.S.: Funding Acquisition; O.R., H.S.: Project Administration; J.T., O.R., and H.S.: Supervision.

Funding Sources

The research leading to these results received funding from the Israel Science Foundation Grant No. 835/23 to H.S. and No. 1266/24 to J.T., and the Stein Family Foundation's support of RNA-seq. H.S. serves as the Senior Academic Advisor to the Azrieli Fellowship-program in Israel. PhD fellowships support was gratefully received the Leopold Sara and Norman Israel fund and the Sephardi Jews Aged Home (to N.M. and S.V.)

Author Disclosures

The authors declare no conflict of interest.

References

- Gill DM. Bacterial toxins: a table of lethal amounts. *Microbiol Rev.* 1982; 46(1):86–94. DOI: [10.1128/mr.46.1.86-94.1982](https://doi.org/10.1128/mr.46.1.86-94.1982). PMID: 6806598; PMCID: [PMC373212](https://pubmed.ncbi.nlm.nih.gov/PMC373212)
- Johnson EA, Montecucco C. Chapter 11 botulism. *Handb Clin Neurol.* 2008;91:333–68. DOI: [10.1097/PCC.0b013e3181c8790c](https://doi.org/10.1097/PCC.0b013e3181c8790c). PMID: 20009784
- Sethi N, Singh S, DeBouille K, Rahman E. A review of complications due to the use of botulinum toxin A for cosmetic indications. *Aesthetic Plast Surg.* 2021;45(3):1210–20. DOI: [10.1007/s00266-020-01983-w](https://doi.org/10.1007/s00266-020-01983-w). PMID: 33051718
- Peck MW. Biology and genomic analysis of *Clostridium botulinum*. *Adv Microb Physiol.* 2009;55:183–320. DOI: [10.1016/S0065-2911\(09\)05503-9](https://doi.org/10.1016/S0065-2911(09)05503-9). PMID: 19573697



5. Pellett S, Yaksh TL, Ramachandran R. Current status and future directions of botulinum neurotoxins for targeting pain processing. *Toxins*. 2015;7(11):4519–63. DOI: [10.3390/toxins7114519](https://doi.org/10.3390/toxins7114519). PMID: 26556371; PMCID: [PMC4663519](https://pubmed.ncbi.nlm.nih.gov/PMC4663519/)
6. Fischer A, Montal M. Crucial role of the disulfide bridge between botulinum neurotoxin light and heavy chains in protease translocation across membranes. *J Biol Chem*. 2007;282(40):29604–11. DOI: [10.1074/jbc.M703619200](https://doi.org/10.1074/jbc.M703619200). PMID: 17666397
7. Schiavo G, Matteoli M, Montecucco C. Neurotoxins affecting neuroexocytosis. *Physiol Rev*. 2000;80(2):717–66. DOI: [10.1152/physrev.2000.80.2.717](https://doi.org/10.1152/physrev.2000.80.2.717). PMID: 10747206
8. Shapiro RL, Hatheway C, Swerdlow DL. Botulism in the United States: a clinical and epidemiologic review. *Ann Intern Med*. 1998;129(3):221–8. DOI: [10.7326/0003-4819-129-3-199808010-00011](https://doi.org/10.7326/0003-4819-129-3-199808010-00011). PMID: 9696731
9. Arnon SS, Chin J. The clinical spectrum of infant botulism. *Rev Infect Dis*. 1979;1(4):614–24. PMID: 7005856
10. Nevas M, Lindström M, Virtanen A, Hielm S, Kuusi M, Arnon SS, et al. Infant botulism acquired from household dust presenting as sudden infant death syndrome. *J Clin Microbiol*. 2005;43(11):511–3. DOI: [10.1128/JCM.43.11.511-513.2005](https://doi.org/10.1128/JCM.43.11.511-513.2005). PMID: 15635031; PMCID: [PMCS40168](https://pubmed.ncbi.nlm.nih.gov/PMCS40168/)
11. Dabritz HA, Friberg IK, Payne JR, Moreno-Gorriñ C, Lunquest K, Thomas D, et al. Elevated incidence of infant botulism in a 17-county area of the Mid-Atlantic region in the United States, 2000–2019, including association with soil types. *Appl Environ Microb*. 2024;90(11), e0106324. DOI: [10.1128/aem.01063-24](https://doi.org/10.1128/aem.01063-24). PMID: 39480097; PMCID: [PMC11577774](https://pubmed.ncbi.nlm.nih.gov/PMC11577774/)
12. Kurokawa Y, Oguma K, Yokosawa N, Syuto B, Fukatsu R, Yamashita I. Binding and cytotoxic effects of Clostridium botulinum type A, C1 and E toxins in primary neuron cultures from foetal mouse brains. *J Gen Microbiol*. 1987;133(9):2647–57. DOI: [10.1099/00221287-133-9-2647](https://doi.org/10.1099/00221287-133-9-2647). PMID: 3329217
13. Peng L, Liu H, Ruan H, Tepp WH, Stoothoff WH, Brown RH, et al. Cytotoxicity of botulinum neurotoxins reveals a direct role of syntaxin 1 and SNAP-25 in neuron survival. *Nat Commun*. 2013;4(1):1472. DOI: [10.1038/ncomms2462](https://doi.org/10.1038/ncomms2462). PMID: 23403573; PMCID: [PMC4052923](https://pubmed.ncbi.nlm.nih.gov/PMC4052923/)
14. Harper CB, Bademosi AT, Coulson EJ, Meunier FA. A role for SNAREs in neuronal survival? *J Neurochem*. 2014;129(5):753–5. DOI: [10.1111/jnc.12699](https://doi.org/10.1111/jnc.12699). PMID: 24697239
15. Ferreira Camargo CH, Ghizoni Teive HA. Use of botulinum toxin for movement disorders. *Drugs Context*. 2019;8:212586. DOI: [10.7573/dic.212586](https://doi.org/10.7573/dic.212586). PMID: 31258617; PMCID: [PMC6586173](https://pubmed.ncbi.nlm.nih.gov/PMC6586173/)
16. Sen E, Kota KP, Panchal RG, Bavari S, Kiris E. Screening of a focused ubiquitin-proteasome pathway inhibitor library identifies small molecules as novel modulators of botulinum neurotoxin type A toxicity. *Front Pharmacol*. 2021;12:763950. DOI: [10.3389/fphar.2021.763950](https://doi.org/10.3389/fphar.2021.763950). PMID: 34646144; PMCID: [PMC8503599](https://pubmed.ncbi.nlm.nih.gov/PMC8503599/)
17. Tsai YC, Kotiy A, Kiris E, Yang M, Bavari S, Tessarollo L, et al. Deubiquitinating enzyme VCIPI135 dictates the duration of botulinum neurotoxin type A intoxication. *Proc Natl Acad Sci U S A*. 2017;114(26):E5158–66. DOI: [10.1073/pnas.1621076114](https://doi.org/10.1073/pnas.1621076114). PMID: 28584101; PMCID: [PMCS495235](https://pubmed.ncbi.nlm.nih.gov/PMCS495235/)
18. Dover JS, Monheit G, Greener M, Pickett A. Botulinum toxin in aesthetic medicine: myths and realities. *Dermatol Surg*. 2017;44(2):249. DOI: [10.1097/DSS.0000000000001277](https://doi.org/10.1097/DSS.0000000000001277). PMID: 29016535; PMCID: [PMC5821482](https://pubmed.ncbi.nlm.nih.gov/PMC5821482/)
19. Ruvkun G. Molecular biology: glimpses of a tiny RNA world. *Science*. 1979;204(5543):797–9. DOI: [10.1126/science.1066315](https://doi.org/10.1126/science.1066315). PMID: 11679654
20. Winek K, Lobentanzer S, Nadorp B, Dubnov S, Dames C, Jagdmann S, et al. Transfer RNA fragments replace microRNA regulators of the cholinergic poststroke immune blockade. *Proc Natl Acad Sci U S A*. 2020;117(51):32606–16. DOI: [10.1073/pnas.2013542117](https://doi.org/10.1073/pnas.2013542117). PMID: 33288717; PMCID: [PMC7768686](https://pubmed.ncbi.nlm.nih.gov/PMC7768686/)
21. Shulman D, Dubnov S, Zorbaz T, Madrer N, Paldor I, Bennett DA, et al. Sex-specific declines in cholinergic-targeting tRNA fragments in the nucleus accumbens in Alzheimer's disease. *Alzheimers Dement*. 2023;19(11):5159–72. DOI: [10.1002/alz.13095](https://doi.org/10.1002/alz.13095). PMID: 37158312; PMCID: [PMC10632545](https://pubmed.ncbi.nlm.nih.gov/PMC10632545/)
22. Dubnov S, Bennett ER, Yayon N, Yakov O, Bennett DA, Seshadri S, et al. Knockout of the longevity gene Klotho perturbs aging and Alzheimer's disease-linked brain microRNAs and tRNA fragments. *Commun Biol*. 2024;7(1):720. DOI: [10.1038/s42003-024-06407-y](https://doi.org/10.1038/s42003-024-06407-y). PMID: 38862813; PMCID: [PMC11166644](https://pubmed.ncbi.nlm.nih.gov/PMC11166644/)
23. Paldor I, Madrer N, Treidel SV, Shulman D, Greenberg DS, Soreq H. Cerebrospinal fluid and blood profiles of transfer RNA fragments show age, sex, and Parkinson's disease-related changes. *J Neurochem*. 2023;164(5):671–83. DOI: [10.1111/jnc.15723](https://doi.org/10.1111/jnc.15723). PMID: 36354307
24. Haussecker D, Huang Y, Lau A, Parameswaran P, Fire AZ, Kay MA. Human tRNA-derived small RNAs in the global regulation of RNA silencing. *RNA*. 2010;16(4):673–95. DOI: [10.1261/rna.2000810](https://doi.org/10.1261/rna.2000810). PMID: 20181738; PMCID: [PMC2844617](https://pubmed.ncbi.nlm.nih.gov/PMC2844617/)
25. Dubnov S, Soreq H. Transfer RNA fragments, from structure to function. *RNA Technologies*. 2023;14:1–19.
26. Cole C, Sobala A, Lu C, Thatcher SR, Bowman A, Brown JWS, et al. Filtering of deep sequencing data reveals the existence of abundant dicer-dependent small RNAs derived from tRNAs. *RNA*. 2009;15(12):2147–60. DOI: [10.1261/rna.1738409](https://doi.org/10.1261/rna.1738409). PMID: 19850906; PMCID: [PMC2779667](https://pubmed.ncbi.nlm.nih.gov/PMC2779667/)
27. Grigoriev A, Karaïskos S. Dynamics of tRNA fragments and their targets in aging mammalian brain. *F1000Res*. 2016;5:2758. DOI: [10.12688/f1000research.10116.1](https://doi.org/10.12688/f1000research.10116.1). PMID: 28105302; PMCID: [PMC5224686](https://pubmed.ncbi.nlm.nih.gov/PMC5224686/)
28. Kumar P, Kuscü C, Dutta A. Biogenesis and function of transfer RNA-related fragments (tRFs). *Trends Biochem Sci*. 2016;41(8):679–89. DOI: [10.1016/j.tibs.2016.05.004](https://doi.org/10.1016/j.tibs.2016.05.004). PMID: 27263052; PMCID: [PMC5173347](https://pubmed.ncbi.nlm.nih.gov/PMC5173347/)
29. Magee R, Rigoutsos I. On the expanding roles of tRNA fragments in modulating cell behavior. *Nucleic Acids Res*. 2020;48(17):9433–48. DOI: [10.1093/nar/gkaa657](https://doi.org/10.1093/nar/gkaa657). PMID: 32890397; PMCID: [PMC7515703](https://pubmed.ncbi.nlm.nih.gov/PMC7515703/)
30. Kim HK, Fuchs G, Wang S, Wei W, Zhang Y, Park H, et al. A transfer-RNA-derived small RNA regulates ribosome biogenesis. *Nature*. 2017;552(7683):57–62. DOI: [10.1038/nature25005](https://doi.org/10.1038/nature25005). PMID: 29186115; PMCID: [PMC6066594](https://pubmed.ncbi.nlm.nih.gov/PMC6066594/)
31. Kuscü C, Kumar P, Kiran M, Su Z, Malik A, Dutta A. tRNA fragments (tRFs) guide ago to regulate gene expression post-transcriptionally in a dicer-independent manner. *RNA*. 2018;24(8):1093–105. DOI: [10.1261/rna.066126.118](https://doi.org/10.1261/rna.066126.118). PMID: 29844106; PMCID: [PMC6049499](https://pubmed.ncbi.nlm.nih.gov/PMC6049499/)
32. Goodarzi H, Liu X, Nguyen HCB, Zhang S, Fish L, Tavazoie SF. Endogenous tRNA-derived fragments suppress breast cancer progression via YBX1 displacement. *Cell*. 2015;161(4):790–802. DOI: [10.1016/j.cell.2015.02.053](https://doi.org/10.1016/j.cell.2015.02.053). PMID: 25957686; PMCID: [PMC4457382](https://pubmed.ncbi.nlm.nih.gov/PMC4457382/)
33. Fagan SG, Helm M, Prehn JHM. tRNA-derived fragments: a new class of non-coding RNA with key roles in nervous system function and dysfunction. *Prog Neurobiol*. 2021;205:102118. DOI: [10.1016/j.pneurobio.2021.102118](https://doi.org/10.1016/j.pneurobio.2021.102118). PMID: 34245849
34. Ivanov P, O'Day E, Emara MM, Wagner G, Lieberman J, Anderson P. G-quadruplex structures contribute to the neuroprotective effects of angiogenin-induced tRNA fragments. *Proc Natl Acad Sci U S A*. 2014;111(51):18201–6. DOI: [10.1073/pnas.1407361111](https://doi.org/10.1073/pnas.1407361111). PMID: 25404306; PMCID: [PMC4280610](https://pubmed.ncbi.nlm.nih.gov/PMC4280610/)
35. Sanadgol N, König L, Drino A, Jovic M, Schaefer MR. Experimental paradigms revisited: oxidative stress-induced tRNA fragmentation does not correlate with stress granule formation but is associated with delayed cell death. *Nucleic Acids Res*. 2022;50(12):6919–37. DOI: [10.1093/nar/gkac495](https://doi.org/10.1093/nar/gkac495). PMID: 35699207; PMCID: [PMC9262602](https://pubmed.ncbi.nlm.nih.gov/PMC9262602/)
36. Xu Y, Zhao J, Zhao Y, Zhou L, Qiao H, Xu Q, et al. The role of ferroptosis in neurodegenerative diseases. *Mol Biol Rep*. 2023;50(2):1655–61. DOI: [10.1007/s11033-022-08048-y](https://doi.org/10.1007/s11033-022-08048-y). PMID: 36385663
37. Ji Y, Zheng K, Li S, Ren C, Shen Y, Tian L, et al. Insight into the potential role of ferroptosis in neurodegenerative diseases. *Front Cell Neurosci*. 2022;16:1005182. DOI: [10.3389/fncel.2022.1005182](https://doi.org/10.3389/fncel.2022.1005182). PMID: 36385946; PMCID: [PMC9647641](https://pubmed.ncbi.nlm.nih.gov/PMC9647641/)
38. Thapa K, Khan H, Kanojia N, Singh TG, Kaur A, Kaur G. Therapeutic insights on ferroptosis in Parkinson's disease. *Eur J Pharmacol*. 2022;930:175133. DOI: [10.1016/j.ejphar.2022.175133](https://doi.org/10.1016/j.ejphar.2022.175133). PMID: 35792170
39. Carlson SE. Docosahexaenoic acid supplementation in pregnancy and lactation. *Am J Clin Nutr*. 2009;89(2):678S–84S. DOI: [10.3945/ajcn.2008.26811E](https://doi.org/10.3945/ajcn.2008.26811E). PMID: 19116324; PMCID: [PMC2647754](https://pubmed.ncbi.nlm.nih.gov/PMC2647754/)
40. Snyder J, Wu Z. Origins of nervous tissue susceptibility to ferroptosis. *Cell Insight*. 2023;2(3):100091. DOI: [10.1016/j.cellin.2023.100091](https://doi.org/10.1016/j.cellin.2023.100091). PMID: 37398634; PMCID: [PMC10308196](https://pubmed.ncbi.nlm.nih.gov/PMC10308196/)
41. Zeng L, Liu Y, Wang Q, Wan H, Meng X, Tu P, et al. Botulinum toxin A attenuates osteoarthritis development via inhibiting chondrocyte ferroptosis through SLC7A11/GPX4 axis. *Biochim Biophys Acta Mol Basis Dis*. 2024;1870(5):167215. DOI: [10.1016/j.bbadis.2024.167215](https://doi.org/10.1016/j.bbadis.2024.167215). PMID: 38714267
42. Jacquemyn J, Ralhan I, Ioannou MS. Driving factors of neuronal ferroptosis. *Trends Cell Biol*. 2024;34(7):535–46. DOI: [10.1016/j.tcb.2024.01.010](https://doi.org/10.1016/j.tcb.2024.01.010). PMID: 38395733
43. Fernández-Salas E, Wang J, Molina Y, Nelson JB, Jacky BPS, Aoki KR. Botulinum neurotoxin serotype a specific cell-based potency assay to replace the mouse bioassay. *PLoS One*. 2012;7(11):e49516. DOI: [10.1371/journal.pone.0049516](https://doi.org/10.1371/journal.pone.0049516). PMID: 23185348; PMCID: [PMC3504020](https://pubmed.ncbi.nlm.nih.gov/PMC3504020/)
44. Wang WC, Lin FM, Chang WC, Lin KY, Huang HD, Lin NS. MiExpress: analyzing high-throughput sequencing data for profiling microRNA expression. *BMC Bioinformatics* 2009;10(1):328. DOI: [10.1186/1471-2105-10-328](https://doi.org/10.1186/1471-2105-10-328). PMID: 19821977; PMCID: [PMC2767369](https://pubmed.ncbi.nlm.nih.gov/PMC2767369/)
45. Loher P, Telonis AG, Rigoutsos I. MINTmap: fast and exhaustive profiling of nuclear and mitochondrial tRNA fragments from short RNA-seq data. *Sci Rep*. 2017;7(1):41184. DOI: [10.1038/srep41184](https://doi.org/10.1038/srep41184). PMID: 28220888; PMCID: [PMC5318995](https://pubmed.ncbi.nlm.nih.gov/PMC5318995/)



46. Lee YS, Shibata Y, Malhotra A, Dutta A. A novel class of small RNAs: tRNA-derived RNA fragments (tRFs). *Genes Dev.* 2009;23(22):2639–49. DOI: [10.1101/gad.1837609](https://doi.org/10.1101/gad.1837609). PMID: 19933153; PMCID: [PMC2779758](https://pubmed.ncbi.nlm.nih.gov/PMC2779758/)
47. Darnell AM, Subramaniam AR, O'Shea EK. Translational control through differential ribosome pausing during amino acid limitation in mammalian cells. *Mol Cell.* 2018;71(2):229–43.e11. DOI: [10.1016/j.molcel.2018.06.041](https://doi.org/10.1016/j.molcel.2018.06.041). PMID: 30029003; PMCID: [PMC6516488](https://pubmed.ncbi.nlm.nih.gov/PMC6516488/)
48. Mao QY, Xie S, Wu LL, Xiang RL, Cai ZG. MicroRNA-mRNA expression profiles and functional network after injection of botulinum toxin type A into sub-mandibular glands. *Toxicol.* 2021;199:31–40. DOI: [10.1016/j.toxicol.2021.05.011](https://doi.org/10.1016/j.toxicol.2021.05.011). PMID: 34052235
49. Maragkakis M, Reczko M, Simossis VA, Alexiou P, Papadopoulos GL, Dalamagas T, et al. DIANA-microT web server: elucidating microRNA functions through target prediction. *Nucleic Acids Res.* 2009;37(suppl_2):W273–6. DOI: [10.1093/nar/gkp292](https://doi.org/10.1093/nar/gkp292). PMID: 19406924; PMCID: [PMC2703977](https://pubmed.ncbi.nlm.nih.gov/PMC2703977/)
50. Kanellos I, Vergoulis T, Sacharidis D, Dalamagas T, Hatzigeorgiou A, Sartze-takis S, et al. MR-microT: a MapReduce-based MicroRNA target prediction method. *ACM International Conference Proceeding Series.* 2014; Available from: <https://dl.acm.org/doi/10.1145/2618243.2618289>
51. Reczko M, Maragkakis M, Alexiou P, Papadopoulos GL, Hatzigeorgiou AG. Accurate microRNA target prediction using detailed binding site accessibility and machine learning on proteomics data. *Front Genet.* 2012;2:17956. DOI: [10.3389/fgene.2011.00103](https://doi.org/10.3389/fgene.2011.00103). PMID: 22303397; PMCID: [PMC3265086](https://pubmed.ncbi.nlm.nih.gov/PMC3265086/)
52. Lobentanzer S, Hanin G, Klein J, Soreq H. Integrative transcriptomics reveals sexually dimorphic control of the cholinergic/neurokinin interface in schizophrenia and bipolar disorder. *Cell Rep.* 2019;29(3):764–77.e5. DOI: [10.1016/j.celrep.2019.09.017](https://doi.org/10.1016/j.celrep.2019.09.017). PMID: 31618642; PMCID: [PMC6899527](https://pubmed.ncbi.nlm.nih.gov/PMC6899527/)
53. Sanadgol N, König L, Drino A, Jovic M, Schaefer MR. Experimental paradigms revisited: oxidative stress-induced tRNA fragmentation does not correlate with stress granule formation but is associated with delayed cell death. *Nucleic Acids Res.* 2022;50(12):6919. DOI: [10.1093/nar/gkac495](https://doi.org/10.1093/nar/gkac495). PMID: 35699207; PMCID: [PMC9262602](https://pubmed.ncbi.nlm.nih.gov/PMC9262602/)
54. Brown AR, Hirschhorn T, Stockwell BR. Ferroptosis-disease perils and therapeutic promise. *Science.* 2024;386(6724):848–9. DOI: [10.1126/science.adn7030](https://doi.org/10.1126/science.adn7030). PMID: 39571009
55. Mortensen MS, Ruiz J, Watts JL. Polyunsaturated fatty acids drive lipid peroxidation during ferroptosis. *Cells.* 2023;12(5):804. DOI: [10.3390/cells12050804](https://doi.org/10.3390/cells12050804). PMID: 36899940; PMCID: [PMC10001165](https://pubmed.ncbi.nlm.nih.gov/PMC10001165/)
56. Crawford RR, Prescott ET, Sylvester CF, Higdon AN, Shan J, Kilberg MS, et al. Human CHAC1 protein degrades glutathione, and mRNA induction is regulated by the transcription factors ATF4 and ATF3 and a bipartite ATF/CRE regulatory element. *J Biol Chem.* 2015;290(25):15878. DOI: [10.1074/jbc.M114.635144](https://doi.org/10.1074/jbc.M114.635144). PMID: 25931127; PMCID: [PMC4505494](https://pubmed.ncbi.nlm.nih.gov/PMC4505494/)
57. Liu Y, Wan Y, Jiang Y, Zhang L, Cheng W. GPX4: the hub of lipid oxidation, ferroptosis, disease and treatment. *Biochim Biophys Acta (BBA).* 2023;1878(3):188890. DOI: [10.1016/j.bbcan.2023.188890](https://doi.org/10.1016/j.bbcan.2023.188890). PMID: 37001616
58. Ray P, Berman JD, Middleton W, Brendle J. Botulinum toxin inhibits arachidonic acid release associated with acetylcholine release from PC12 cells. *J Biol Chem.* 1993;268(15):11057–64. PMID: 8496167
59. Yu Y, Ren Y, Wang C, Li Z, Niu F, Li Z, et al. Arginase 2 negatively regulates sorafenib-induced cell death by mediating ferroptosis in melanoma: the role of Arginase 2 in sorafenib-induced ferroptosis in melanoma. *Acta Biochim Biophys Sin (Shanghai).* 2022;54(11):1658. DOI: [10.3724/abbs.2022166](https://doi.org/10.3724/abbs.2022166). PMID: 36604146; PMCID: [PMC9828469](https://pubmed.ncbi.nlm.nih.gov/PMC9828469/)
60. Gao M, Monian P, Quadri N, Ramasamy R, Jiang X. Glutaminolysis and transferin regulate ferroptosis. *Mol Cell.* 2015;59(2):298–308. DOI: [10.1016/j.molcel.2015.06.011](https://doi.org/10.1016/j.molcel.2015.06.011). PMID: 26166707; PMCID: [PMC4506736](https://pubmed.ncbi.nlm.nih.gov/PMC4506736/)
61. Hou W, Xie Y, Song X, Sun X, Lotze MT, Zeh HJ, et al. Autophagy promotes ferroptosis by degradation of ferritin. *Autophagy.* 2016;12(8):1425–8. DOI: [10.1080/15548627.2016.1187366](https://doi.org/10.1080/15548627.2016.1187366). PMID: 27245739; PMCID: [PMC4968231](https://pubmed.ncbi.nlm.nih.gov/PMC4968231/)
62. Clément T, Salone V, Rederstorff M. Dual luciferase gene reporter assays to study miRNA function. *Methods Mol Biol.* 2015;1296:187–98. DOI: [10.1007/978-1-4939-2547-6_17](https://doi.org/10.1007/978-1-4939-2547-6_17). PMID: 25791601
63. Harvey SE, Xu Y, Lin X, Gao XD, Qiu Y, Ahn J, et al. Coregulation of alternative splicing by hnRNP and ESRP1 during EMT. *RNA.* 2018;24(10):1326–38. DOI: [10.1261/rna.066712.118](https://doi.org/10.1261/rna.066712.118). PMID: 30042172; PMCID: [PMC6140460](https://pubmed.ncbi.nlm.nih.gov/PMC6140460/)
64. Zhang G, Neubert TA, Jordan BA. RNA binding proteins accumulate at the post-synaptic density with synaptic activity. *J Neurosci.* 2012;32(2):599–609. DOI: [10.1523/JNEUROSCI.2463-11.2012](https://doi.org/10.1523/JNEUROSCI.2463-11.2012). PMID: 22238095; PMCID: [PMC3561928](https://pubmed.ncbi.nlm.nih.gov/PMC3561928/)
65. Zheng R, Dunlap M, Bobkov GOM, Gonzalez-Figueroa C, Patel KJ, Lyu J, et al. hnRNP protects against the dsRNA-mediated interferon response by repressing LINE-associated cryptic splicing. *Mol Cell.* 2024;84(11):2087–103.e8. DOI: [10.1016/j.molcel.2024.05.004](https://doi.org/10.1016/j.molcel.2024.05.004). PMID: 38815579; PMCID: [PMC11204102](https://pubmed.ncbi.nlm.nih.gov/PMC11204102/)
66. Miao M, Wang Y, Zeng S, Han Y, Zhu R, Yu P, et al. Identification and validation of ferroptosis-related genes in Sevoflurane-induced hippocampal neurotoxicity. *Oxid Med Cell Longev.* 2022;2022(1):4435161. DOI: [10.1155/2022/4435161](https://doi.org/10.1155/2022/4435161). PMID: 36238640; PMCID: [PMC9553355](https://pubmed.ncbi.nlm.nih.gov/PMC9553355/)
67. Wang J, Luo X, Liu D. Knockdown of HNRNPM inhibits the progression of glioma through inducing ferroptosis. *Cell Cycle.* 2023;22(20):2264–79. DOI: [10.1080/15384101.2023.2286782](https://doi.org/10.1080/15384101.2023.2286782). PMID: 38016815; PMCID: [PMC10730218](https://pubmed.ncbi.nlm.nih.gov/PMC10730218/)
68. Madrer N, Vaknine-Treidel S, Zorbaz T, Tzur Y, Drori P, Greenberg DS, et al. Pre-symptomatic Parkinson's disease qPCR-based Blood test detecting a conserved sequence motif in transfer RNA fragments. *Nat Aging.* 2025.
69. Bartel DP. Metazoan microRNAs. *Cell.* 2018;173(1):20–51. DOI: [10.1016/j.cell.2018.03.006](https://doi.org/10.1016/j.cell.2018.03.006). PMID: 29570994; PMCID: [PMC6091663](https://pubmed.ncbi.nlm.nih.gov/PMC6091663/)
70. Brenner S. The genetics of caenorhabditis elegans. *Genetics.* 1974;77(1):71–94. DOI: [10.1093/genetics/77.1.71](https://doi.org/10.1093/genetics/77.1.71). PMID: 4366476; PMCID: [PMC1213120](https://pubmed.ncbi.nlm.nih.gov/PMC1213120/)
71. Poon VY, Klassen MP, Shen K. UNC-6/netrin and its receptor UNC-5 locally exclude presynaptic components from dendrites. *Nature.* 2008;455(7213):669–73. DOI: [10.1038/nature07291](https://doi.org/10.1038/nature07291). PMID: 18776887; PMCID: [PMC3912858](https://pubmed.ncbi.nlm.nih.gov/PMC3912858/)
72. Ma L, Pan L, Liu W, Liu Y, Xiang X, Pan Y, et al. Agrin influences botulinum neurotoxin A-induced nerve sprouting via miR-144-agrin-MuSK signaling. *Front Cell Dev Biol.* 2020;8:15. DOI: [10.3389/fcell.2020.00015](https://doi.org/10.3389/fcell.2020.00015). PMID: 32083076; PMCID: [PMC7003618](https://pubmed.ncbi.nlm.nih.gov/PMC7003618/)
73. Tomas J, Lanuza M, Santafe M, Fenoll-Brunetand Garcia MN. Topological differences along mammalian motor nerve terminals for spontaneous and alpha-bungarotoxin-induced sprouting. *Histol Histopathol.* 2000;15(1):43–52. DOI: [10.14670/HH-15.43](https://doi.org/10.14670/HH-15.43). PMID: 10668194
74. Bhat SA, Gurtoo S, Deolankar SC, Fazili KM, Advani J, Shetty R, et al. A network map of netrin receptor UNC5B-mediated signaling. *J Cell Commun Signal.* 2019;13(1):121–7. DOI: [10.1007/s12079-018-0485-z](https://doi.org/10.1007/s12079-018-0485-z). PMID: 30084000; PMCID: [PMC6381369](https://pubmed.ncbi.nlm.nih.gov/PMC6381369/)
75. Pellett S, Bradshaw M, Tepp WH, Pier CL, Whitmarsh RCM, Chen C, et al. The light chain defines the duration of action of botulinum toxin serotype a subtypes. *mBio.* 2018;9(2):e00089–18. DOI: [10.1128/mBio.00089-18](https://doi.org/10.1128/mBio.00089-18). PMID: 29588398; PMCID: [PMC5874905](https://pubmed.ncbi.nlm.nih.gov/PMC5874905/)
76. Tsai YC, Maditz R, Kuo CL, Fishman PS, Shoemaker CB, Oyler GA, et al. Targeting botulinum neurotoxin persistence by the ubiquitin-proteasome system. *Proc Natl Acad Sci U S A.* 2010;107(38):16554–9. DOI: [10.1073/pnas.1008302107](https://doi.org/10.1073/pnas.1008302107). PMID: 20823219; PMCID: [PMC2944746](https://pubmed.ncbi.nlm.nih.gov/PMC2944746/)
77. Tzur Y, Winek K, Madrer N, Dubnov S, Bennett ER, Greenberg DS, et al. Lysine tRNA fragments and miR-194-5p co-regulate hepatic steatosis via β -klotho and perilipin 2. *Mol Metab.* 2024;79:101856. DOI: [10.1016/j.molmet.2023.101856](https://doi.org/10.1016/j.molmet.2023.101856). PMID: 38141848; PMCID: [PMC10805669](https://pubmed.ncbi.nlm.nih.gov/PMC10805669/)
78. Ohno K, Ohkawara B, Shen XM, Selcen D, Engel AG. Clinical and pathologic features of congenital myasthenic syndromes caused by 35 genes—a comprehensive review. *Int J Mol Sci.* 2023;24(4):3730. DOI: [10.3390/ijms24043730](https://doi.org/10.3390/ijms24043730). PMID: 36835142; PMCID: [PMC9961056](https://pubmed.ncbi.nlm.nih.gov/PMC9961056/)
79. Scherf JM, Hu XS, Tepp WH, Ichtchenko K, Johnson EA, Pellett S. Analysis of gene expression in induced pluripotent stem cell-derived Human neurons exposed to botulinum neurotoxin A subtype 1 and a type A atoxic derivative. *PLoS One.* 2014;9(10):e111238. DOI: [10.1371/journal.pone.0111238](https://doi.org/10.1371/journal.pone.0111238). PMID: 25337697; PMCID: [PMC4206481](https://pubmed.ncbi.nlm.nih.gov/PMC4206481/)
80. Wang L, Ringelberg CS, Singh BR. Dramatic neurological and biological effects by botulinum neurotoxin type A on SH-SY5Y neuroblastoma cells, beyond the blockade of neurotransmitter release. *BMC Pharmacol Toxicol.* 2020;21(1):66. DOI: [10.1186/s40360-020-00443-0](https://doi.org/10.1186/s40360-020-00443-0). PMID: 32891179; PMCID: [PMC7487822](https://pubmed.ncbi.nlm.nih.gov/PMC7487822/)
81. Valois LS, Shi VH, Bishop P, Zhu B, Nakamura Y, Wilkinson KA, et al. Neurotrophic effects of Botulinum neurotoxin type A in hippocampal neurons involve activation of Rac1 by the non-catalytic heavy chain (HCC/A). *IBRO Neurosci Rep.* 2021;10:196–207. DOI: [10.1016/j.ibneur.2021.04.002](https://doi.org/10.1016/j.ibneur.2021.04.002). PMID: 34041508; PMCID: [PMC8143998](https://pubmed.ncbi.nlm.nih.gov/PMC8143998/)
82. Kim S, Larrous F, Varet H, Legendre R, Feige L, Dumas G, et al. Early transcriptional changes in rabies virus-infected neurons and their impact on neuronal functions. *Front Microbiol.* 2021;12:730892. DOI: [10.3389/fmicb.2021.730892](https://doi.org/10.3389/fmicb.2021.730892). PMID: 34970230; PMCID: [PMC8713068](https://pubmed.ncbi.nlm.nih.gov/PMC8713068/)
83. Brandão-Teles C, Antunes ASLM, de MoraesVrechi TA, Martins-de-Souza D. The roles of hnRNP family in the brain and brain-related disorders. *Mol Neurobiol.* 2023;61(6):3578–95. DOI: [10.1007/s12035-023-03747-4](https://doi.org/10.1007/s12035-023-03747-4). PMID: 37999871
84. Luo Y, Yao M, Wang R, Liao S, Yu J. Netrin-1 binding to UNC5b improves post-stroke neuronal ferroptosis via AMPK-BACH1 pathway. *Eur J Pharmacol.* 2025;985:177507. DOI: [10.1016/j.ejphar.2025.177507](https://doi.org/10.1016/j.ejphar.2025.177507). PMID: 40086580
85. Sun Y, Xia X, Basnet D, Zheng JC, Huang J, Liu J. Mechanisms of ferroptosis and emerging links to the pathology of neurodegenerative diseases. *Front Aging Neurosci.* 2022;14:904152. DOI: [10.3389/fnagi.2022.904152](https://doi.org/10.3389/fnagi.2022.904152). PMID: 35837484; PMCID: [PMC9273851](https://pubmed.ncbi.nlm.nih.gov/PMC9273851/)



86. Dixon SJ, Olzmann JA. The cell biology of ferroptosis. *Nat Rev Mol Cell Biol.* 2024;25(6):424–42. DOI: [10.1038/s41580-024-00703-5](https://doi.org/10.1038/s41580-024-00703-5). PMID: 38366038
87. Tang H, Kang R, Liu J, Tang D. ATF4 in cellular stress, ferroptosis, and cancer. *Arch Toxicol.* 2024;98(4):1025–41. DOI: [10.1007/s00204-024-03681-x](https://doi.org/10.1007/s00204-024-03681-x). PMID: 38383612
88. Mungrue IN, Pagnon J, Kohannim O, Gargalovic PS, Lusis AJ. CHAC1/MGC4504 Is a novel proapoptotic component of the unfolded protein response, downstream of the ATF4-ATF3-CHOP cascade. *J Immunol.* 2009;182(1):466–76. DOI: [10.4049/jimmunol.182.1.466](https://doi.org/10.4049/jimmunol.182.1.466). PMID: 19109178; PMCID: [PMC2846782](https://pubmed.ncbi.nlm.nih.gov/PMC2846782/)
89. Du Y, Guo Z. Recent progress in ferroptosis: inducers and inhibitors. *Cell Death Discov.* 2022;8(1):501. DOI: [10.1038/s41420-022-01297-7](https://doi.org/10.1038/s41420-022-01297-7). PMID: 36581640; PMCID: [PMC9800531](https://pubmed.ncbi.nlm.nih.gov/PMC9800531/)
90. Nestor MS, Arnold D, Fischer D. The mechanisms of action and use of botulinum neurotoxin type A in aesthetics: key clinical postulates II. *J Cosmet Dermatol.* 2020;19(11):2785–804. DOI: [10.1111/jocd.13702](https://doi.org/10.1111/jocd.13702). PMID: 32866999; PMCID: [PMC7693297](https://pubmed.ncbi.nlm.nih.gov/PMC7693297/)
91. Bray NL, Pimentel H, Melsted P, Pachter L. Near-optimal probabilistic RNA-seq quantification. *Nat Biotechnol.* 2016;34(5):525–7. DOI: [10.1038/nbt.3519](https://doi.org/10.1038/nbt.3519). PMID: 27043002
92. GitHub - s-andrews/FastQC: a quality control analysis tool for high throughput sequencing data. 2022. Available from: <https://github.com/s-andrews/FastQC>
93. Dodd M, Roehr JT, Ahmed R, Dieterich C. FLEXBAR—Flexible barcode and adapter processing for next-generation sequencing platforms. *Biology (Basel).* 2012;1(3):895–905. DOI: [10.3390/biology1030895](https://doi.org/10.3390/biology1030895). PMID: 24832523; PMCID: [PMC4009805](https://pubmed.ncbi.nlm.nih.gov/PMC4009805/)
94. Robinson MD, McCarthy DJ, Smyth GK. edgeR: a bioconductor package for differential expression analysis of digital gene expression data. *Bioinformatics.* 2010;26(1):139–40. DOI: [10.1093/bioinformatics/btp616](https://doi.org/10.1093/bioinformatics/btp616). PMID: 19910308; PMCID: [PMC2796818](https://pubmed.ncbi.nlm.nih.gov/PMC2796818/)
95. Hinden L, Ahmad M, Hamad S, Nemirovski A, Szanda G, Glasmacher S, et al. Opposite physiological and pathological mTORC1-mediated roles of the CB1 receptor in regulating renal tubular function. *Nat Commun.* 2022;13(1):1783. DOI: [10.1038/s41467-022-29124-8](https://doi.org/10.1038/s41467-022-29124-8). PMID: 35379807; PMCID: [PMC8980033](https://pubmed.ncbi.nlm.nih.gov/PMC8980033/)
96. MacKay GM, Zheng L, Van Den Broek NJF, Gottlieb E. Analysis of cell metabolism using LC-MS and isotope tracers. *Methods Enzymol.* 2015;561:171–96. DOI: [10.1016/bs.mie.2015.05.016](https://doi.org/10.1016/bs.mie.2015.05.016). PMID: 26358905
97. Kim H, Xue X. Detection of total reactive oxygen species in adherent cells by 2',7'-dichlorodihydrofluorescein diacetate staining. *J Vis Exp.* 2020. DOI: [10.3791/60682](https://doi.org/10.3791/60682). PMID: 32658187; PMCID: [PMC7712457](https://pubmed.ncbi.nlm.nih.gov/PMC7712457/)
98. Bailey TL, Johnson J, Grant CE, Noble WS. The MEME Suite. *Nucleic Acids Res.* 2015;43(W1):W39–49. DOI: [10.1093/nar/gkv416](https://doi.org/10.1093/nar/gkv416). PMID: 25953851; PMCID: [PMC4489269](https://pubmed.ncbi.nlm.nih.gov/PMC4489269/)
99. Li N, Shan N, Lu L, Wang Z. tRFtarget: a database for transfer RNA-derived fragment targets. *Nucleic Acids Res.* 2021;49(D1):D254–60. DOI: [10.1093/nar/gkaa831](https://doi.org/10.1093/nar/gkaa831). PMID: 33035346; PMCID: [PMC7779015](https://pubmed.ncbi.nlm.nih.gov/PMC7779015/)
100. Li N, Yao S, Yu G, Lu L, Wang Z. tRFtarget 2.0: expanding the targetome landscape of transfer RNA-derived fragments. *Nucleic Acids Res.* 2024;52(D1):D345–50. DOI: [10.1093/nar/gkad815](https://doi.org/10.1093/nar/gkad815). PMID: 37811890; PMCID: [PMC10767876](https://pubmed.ncbi.nlm.nih.gov/PMC10767876/)

Publisher's note: Genomic Press maintains a position of impartiality and neutrality regarding territorial assertions represented in published materials and affiliations of institutional nature. As such, we will use the affiliations provided by the authors, without editing them. Such use simply reflects what the authors submitted to us and it does not indicate that Genomic Press supports any type of territorial assertions.



Open Access. This article is licensed to Genomic Press under the Creative Commons Attribution-NonCommercial-NoDerivatives 4.0 International License (CC BY-NC-ND 4.0). The license mandates: (1) Attribution: Credit must be given to the original work, with a link to the license and notification of any changes. The acknowledgment should not imply licensor endorsement. (2) NonCommercial: The material cannot be used for commercial purposes. (3) NoDerivatives: Modified versions of the work cannot be distributed. (4) No additional legal or technological restrictions may be applied beyond those stipulated in the license. Public domain materials or those covered by statutory exceptions are exempt from these terms. This license does not cover all potential rights, such as publicity or privacy rights, which may restrict material use. Third-party content in this article falls under the article's Creative Commons license unless otherwise stated. If use exceeds the license scope or statutory regulation, permission must be obtained from the copyright holder. For complete license details, visit <https://creativecommons.org/licenses/by-nc-nd/4.0/>. The license is provided without warranties.